Check for updates

ADVANCING EARTH AND SPACE SCIENCES

JGR Solid Earth

RESEARCH ARTICLE

10.1029/2024JB029036

Key Points:

- Paleomagnetic directions from mafic sills in Death Valley are consistent with ca. 1,098 Ma LIP-style magmatism in southwestern Laurentia
- A paleomagnetic pole from the ca. 1,082 Ma Cardenas Basalt of the Grand Canyon corresponds with time-equivalent Midcontinent Rift poles
- Changing southwestern Laurentia LIP pole positions support rapid equatorward motion of the continent recorded by the Keweenawan Track

Supporting Information:

Supporting Information may be found in the online version of this article.

Correspondence to:

Y. Zhang,
yiming-z@umn.edu

Citation:

Zhang, Y., Anderson, N. S., Mohr, M. T., Nelson, L. L., Macdonald, F. A., Schmitz, M. D., et al. (2024). Paleomagnetic records from pulsed magmatism in the southwestern Laurentia large igneous province and Cardenas Basalt support rapid late Mesoproterozoic plate motion. *Journal of Geophysical Research: Solid Earth*, *129*, e2024JB029036. https://doi.org/10.1029/2024JB029036

Received 4 MAR 2024
Accepted 28 SEP 2024

Author Contributions:

Conceptualization: Yiming Zhang, Nicolas S. Anderson, Nicholas L. Swanson-Hysell
Data curation: Yiming Zhang, Nicolas S. Anderson
Formal analysis: Yiming Zhang, Nicolas S. Anderson, Nicholas L. Swanson-Hysell
Funding acquisition: Yiming Zhang, Nicolas S. Anderson, Nicholas L. Swanson-Hysell
Investigation: Yiming Zhang, Nicolas S. Anderson, Nicholas L. Swanson-Hysell
Methodology: Yiming Zhang, Nicolas S. Anderson, Nicholas L. Swanson-Hysell

© 2024. The Author(s).
This is an open access article under the terms of the Creative Commons Attribution License, which permits use, distribution and reproduction in any medium, provided the original work is properly cited.

Paleomagnetic Records From Pulsed Magmatism in the Southwestern Laurentia Large Igneous Province and Cardenas Basalt Support Rapid Late Mesoproterozoic Plate Motion

Yiming Zhang[1,2], Nicolas S. Anderson[2,3], Michael T. Mohr[4], Lyle L. Nelson[5], Francis A. Macdonald[2,6], Mark D. Schmitz[4], Olivia G. Thurston[7], William R. Guenthner[7], Karl E. Karlstrom[8], and Nicholas L. Swanson-Hysell[1,2]

[1]Department of Earth and Environmental Sciences, Institute for Rock Magnetism, University of Minnesota, Minneapolis, MN, USA, [2]Department of Earth and Planetary Science, University of California, Berkeley, CA, USA, [3]Division of Geological and Planetary Sciences, California Institute of Technology, Pasadena, CA, USA, [4]Department of Geoscience, Boise State University, Boise, ID, USA, [5]Department of Earth, Atmospheric & Planetary Sciences, MIT, Cambridge, MA, USA, [6]Department of Earth Science, University of California, Santa Barbara, CA, USA, [7]Department of Geology, University of Illinois at Urbana-Champaign, Urbana, IL, USA, [8]Department of Earth and Planetary Sciences, University of New Mexico, Albuquerque, NM, USA

Abstract Mafic intrusions, lava flows, and felsic plutons in southwestern Laurentia have been hypothesized to be associated with the emplacement of a late Mesoproterozoic (Stenian Period) large igneous province. Improved geochronologic data resolve distinct episodes of mafic magmatism in the region. The ca. 1,098 Ma main pulse of southwestern Laurentia large igneous province (SWLLIP) magmatism is recorded by mafic intrusions across southeastern California to central Arizona. A younger episode of volcanism resulted in eruptions that formed the ca. 1,082 Ma Cardenas Basalt, which is the uppermost unit of the Unkar Group in the Grand Canyon. With the updated geochronological constraints, we develop new paleomagnetic data from mafic sills in the SWLLIP. Overlapping poles between the Death Valley sills and rocks of similar age in the Midcontinent Rift are inconsistent with large-scale Cenozoic vertical axis rotations in Death Valley. We also develop a new paleomagnetic pole from the ca. 1,082 Ma Cardenas Basalt (pole longitude = 183.9°E, pole latitude = 15.9°N, A_{95} = 7.4°, N = 18). The new paleomagnetic data are consistent with the pole path developed from time-equivalent rocks of the Midcontinent Rift, supporting interpretations that changing pole positions are the result of rapid equatorward motion. These data add to the record of Laurentia's rapid motion from ca. 1,110 to 1,080 Ma that culminated in collisional Grenvillian orogenesis and the assembly of Rodinia.

Plain Language Summary In Earth's geological record, voluminous magmatism over brief time frames are known as large igneous provinces. One such event took place approximately 1.1 billion years ago on the ancient North American continent (known as Laurentia) resulting in the formation of thick mafic sills. Previously, these intrusions across southwestern Laurentia were believed to have been emplaced simultaneously with the extrusive Cardenas Basalt lava flows in the Grand Canyon. We now know that the emplacement of the thick mafic intrusions represent a large igneous province, which predates the eruption of the Cardenas Basalt by 16 million years. By pairing this knowledge of the age with recorded magnetic directions in the lavas and intrusions, we can enrich our knowledge of Laurentia's motion leading up to the assembly of the supercontinent Rodinia. These data provide a new constraint on the position of the continent 1,082 million years ago and support the interpretation of rapid plate motion over the preceding 20 million years.

1. Introduction

The ancient North American craton (Laurentia) has a rich record of Stenian (late Mesoproterozoic) mafic magmatism. In the Midcontinent Rift of the Lake Superior region, punctuated episodes of voluminous intrusions and associated volcanism have been dated between 1,109 and 1,084 Ma with high-precision geochronology (Figure 1). Paleomagnetic data from these well-preserved and well-dated rocks within the Midcontinent Rift make up the majority of the Stenian database of paleomagnetic poles for Laurentia (Evans et al., 2021). These data provide central constraints on global paleogeography during the assembly of supercontinent Rodinia (Evans, 2021; Swanson-Hysell, 2021).

Project administration: Karl E. Karlstrom, Nicholas L. Swanson-Hysell
Resources: Yiming Zhang, Nicolas S. Anderson, Michael T. Mohr, Lyle L. Nelson, Francis A. Macdonald, Mark D. Schmitz, Olivia G. Thurston, William R. Guenthner, Karl E. Karlstrom, Nicholas L. Swanson-Hysell
Software: Yiming Zhang, Nicolas S. Anderson, Nicholas L. Swanson-Hysell
Supervision: Karl E. Karlstrom, Nicholas L. Swanson-Hysell
Visualization: Yiming Zhang, Nicolas S. Anderson, Lyle L. Nelson, Francis A. Macdonald, Nicholas L. Swanson-Hysell
Writing – original draft: Yiming Zhang, Nicolas S. Anderson
Writing – review & editing: Yiming Zhang, Michael T. Mohr, Lyle L. Nelson, Francis A. Macdonald, Nicholas L. Swanson-Hysell

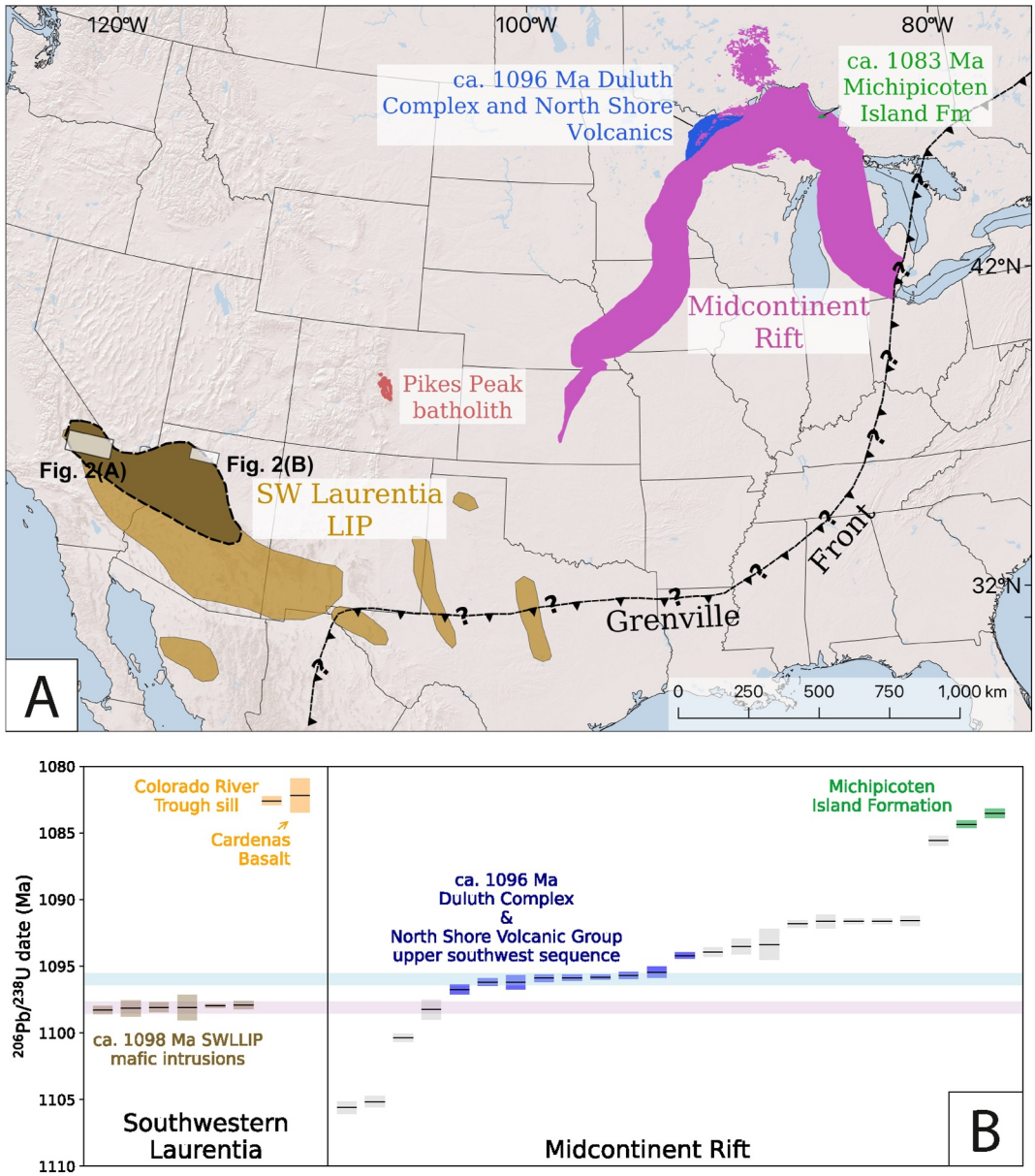

Figure 1. (a) Map of North America showing the inferred extent of the southwestern Laurentia large igneous province (SWLLIP) modified from Bright et al. (2014) in light brown color, a more strict version of the inferred extent of the SWLLIP based on encircling sills dated to be ca. 1,098 Ma through the high-precision geochronology data of Mohr et al. (2024) in dark brown, together with the Pikes Peak batholith (Green, 1992), and the inferred extent of the Midcontinent Rift. The inferred trace of the Grenville Front is modified from Rivers (2015). The inset boxes show the extent of maps in Figure 2. (b) Summary of high-precision zircon U-Pb geochronology data from southwestern Laurentia (Mohr et al., 2024) and from the Midcontinent Rift, highlighting the ca. 1,096 Ma Duluth Complex and the associated North Shore Volcanic Group (Swanson-Hysell et al., 2019, 2021) and the ca. 1,084 Ma Michipicoten Island Formation (Fairchild et al., 2017). The 1,082.6 ± 0.3 Ma Colorado River Trough sill is located in the Dead Mountains in southeastern California (Mohr et al., 2024). Each black bar represents a $^{206}Pb/^{238}U$ zircon weighted mean age. The colored shaded regions associated with the black bars represent uncertainties of the mean ages at 95% confidence level calculated with a Student's-T multiplier.

In southwestern Laurentia, widespread Stenian magmatism led to the emplacement of mafic intrusions and lava flows as well as felsic plutons (Figure 1a; Bright et al., 2014; Hendricks, 1972; Howard, 1991; Shride, 1967; Wrucke, 1966). Based on petrologic and geochemical data (e.g., Hammond, 1986; Wrucke, 1966; Wrucke & Shride, 1972), it was previously suggested that the mafic intrusions in the region were contemporaneous. However, in comparison to the Midcontinent Rift where extensive high-precision zircon U-Pb geochronology

21699356, 2024, 10, Downloaded from https://agupubs.onlinelibrary.wiley.com/doi/10.1029/2024JB029036 by Yiming Zhang - University Of Minnesota Lib , Wiley Online Library on [19/10/2024]. See the Terms and Conditions (https://onlinelibrary.wiley.com/terms-and-conditions) on Wiley Online Library for rules of use; OA articles are governed by the applicable Creative Commons License

data have been developed (typically with analytical uncertainties <1 Myr; e.g. Swanson-Hysell et al., 2019), most ages from rocks associated with the Stenian southwestern Laurentia magmatism have been relatively imprecise (e.g., as compiled and developed in Bright et al. (2014)). The broadly overlapping ages, albeit with large uncertainties, of rocks that outcrop in California, Arizona, New Mexico, and Mexico led Bright et al. (2014) to hypothesize that they could be grouped as the southwestern Laurentia large igneous province (SWLLIP). Bright et al. (2014) further suggested that a temporal overlap of magmatism in the SWLLIP and in the Midcontinent Rift was the result of a geodynamic linkage. However, the available geochronology data from the SWLLIP at the time was not precise enough to test its relationship with the magmatic events in the Midcontinent Rift.

Due to sparse geochronology data, temporal relationships between units in southwestern Laurentia are mostly inferred. In the Grand Canyon, it has been hypothesized that thick mafic sills and dikes that intrude Unkar Group sedimentary rocks are feeder systems for the Cardenas Basalt lava flows which are the uppermost unit of the Unkar Group (e.g., Hammond & Wooden, 1990; Larson et al., 1994; Timmons et al., 2005). This hypothesis is based on the spatial proximity of the units as well as similarities in trace and major element concentrations of lava flows and a limited number of nearby intrusions (Larson et al., 1994). No direct field evidence exists for feeder relations. Hendricks (1989) considered the sills and flows to be from the same parent magma, but did discuss a possible interpretation that the more evolved flows erupted later than the emplacement of the sills. Applying the assumption that the extrusive and intrusive rocks were coeval, Weil et al. (2003) developed a paleomagnetic pole by grouping data derived from 13 mafic intrusions and three Cardenas Basalt lava flows in the Grand Canyon. Similar directions had previously been developed for two Cardenas lava flows by Elston and Scott (1973). Weil et al. (2003) assigned an age of 1,090.6 ± 4.5 Ma (2σ) to their pole based on an ^{40}Ar-^{39}Ar age they developed from biotite interpreted to have formed within the host Unkar sedimentary rocks during the intrusion of a mafic sill.

Paleomagnetic data have also been developed from SWLLIP mafic sills that intrude Apache Group sedimentary rocks in central Arizona (Donadini et al., 2011; Harlan, 1993; Helsley & Spall, 1972). These studies interpreted sills with normal-polarity paleomagnetic directional data as coeval. Donadini et al. (2011) developed a mean pole from some normal-polarity sills and considered the age of the pole to be that of a baddeleyite U-Pb age of 1,088 ± 11 Ma (2σ; age from one sill later published by Bright et al., 2014). Although Harlan (1993) also obtained paleomagnetic samples of mafic sills in the same region with clearer distinction between individual cooling units, that the normal paleomagnetic pole of Donadini et al. (2011) was reported with a paired radiometric age assignment led it to be the pole that is included in recent curated compilations (e.g., Evans et al., 2021). Other sills in the region record reversed directions with steeper inclinations relative to the normal polarity directions (Donadini et al., 2011; Harlan, 1993). In the field guide of Donadini et al. (2012), an age of 1,119 ± 10 Ma (weighted mean of ^{207}Pb/^{206}Pb age of 2 baddeleyite grains) and an age of 1,111.6 ± 8.9 Ma (concordia intercept age of a combination of baddeleyite and zircon dates) were reported for sills of reversed polarity—these geochronology data remain unpublished. Both the steeply reversed directions and the geochronological data are consistent with these sills being emplaced during an interval of reversed polarity prior to or during ca. 1,109 to 1,105 Ma early stage Midcontinent Rift magmatism (Swanson-Hysell et al., 2019; Vervoort et al., 2007).

More recently, Mohr et al. (2024) developed chemical abrasion-isotope dilution-thermal ionization mass spectrometry (CA-ID-TIMS) high-precison U-Pb geochronology data from zircon separated from coarse-grained interior of a thick lava flow within the Cardenas Basalt (Figure 4) (applying the approach of Oliveira et al., 2022). Three sills in Death Valley were dated at 1,097.91 ± 0.29 Ma, 1,098.27 ± 0.27 Ma, and 1,098.09 ± 0.91 Ma, two sills in western Grand Canyon at 1,098.16 ± 0.59 Ma and 1,098.09 ± 0.34 Ma, and one sill in central Arizona at 1,097.97 ± 0.12 Ma (all ages are presented with analytical uncertainties at 95% confidence which is calculated including a Student's-T multiplier; Mohr et al., 2024). These ages agree with each other within uncertainty (Figure 1b) and suggest that the mafic intrusions across the region were rapidly emplaced in ~0.25 Myr (Mohr et al., 2024). The data indicate an episode of LIP style mafic magmatism ca. 1,098 Ma in southwestern Laurentia that postdates the early plateau stage of volcanism in the Midcontinent Rift (ca. 1,104–1,098 Ma; Miller & Nicholson, 2013; Vervoort et al., 2007) and predates the emplacement of the ca. 1,096 Ma Duluth Complex and thick main stage rift volcanics (Figure 1). The data are consistent with a model where a plume head arrived ca. 1,098 Ma under southwestern Laurentia leading to generation of melt and the emplacement of thick mafic intrusions. This plume could have then spread along the base of the lithosphere toward the Midcontinent Rift where it facilitated the reinvigoration of magmatism associated with the emplacement of the Duluth Complex and the North Shore Volcanic Group (Mohr et al., 2024). In addition, Mohr et al. (2024) developed a new zircon U-Pb age

21699356, 2024, 10, Downloaded from https://agupubs.onlinelibrary.wiley.com/doi/10.1029/2024JB029036 by Yiming Zhang - University Of Minnesota Lib , Wiley Online Library on [19/10/2024]. See the Terms and Conditions (https://onlinelibrary.wiley.com/terms-and-conditions) on Wiley Online Library for rules of use; OA articles are governed by the applicable Creative Commons License

of 1,082.18 ± 1.25 Ma (95% confidence) from a Cardenas Basalt lava flow. That age indicates that the eruption of the lavas postdated the widespread ca. 1,098 Ma mafic intrusions by ~16 Myr (Figure 1b). Given the rapid apparent polar wander shown by the ca. 1,109–1,080 Ma Keweenawan Track (Swanson-Hysell et al., 2019), the ~16 Myr age difference between the Cardenas Basalt and thick mafic sills leads to the prediction that the units should record distinct paleomagnetic pole positions separated by a large angular distance.

In this study, we develop new paleomagnetic data from the dated mafic sills and additional undated Mesoproterozoic intrusions in Death Valley and the Grand Canyon. We also develop new paleomagnetic data from 18 lava flows of the Cardenas Basalt within the Grand Canyon with volcanostratigraphic context. Paired with the new high-precision geochronology data, our new paleomagnetic data help clarify the current known extent of the ca. 1,098 Ma southwestern Laurentia large igneous province. The ca. 1,082 Ma Cardenas Basalt paleomagnetic pole can be incorporated into analyses of the Phanerozoic deformation history of the Colorado Plateau, and adds a new reliable constraint on Laurentia's late Mesoproterozoic apparent polar wander path.

2. Geological Background

2.1. Mafic Intrusions in the Crystal Spring Formation, Death Valley

Rocks in the Death Valley region record the geological evolution of the southwestern margin of Laurentia since ca. 1.8 Ga in the Paleoproterozoic Era (Tapani Rämö & Calzia, 1998; Figures 2a and 3). The basement rocks include Paleoproterozoic para- and orthogneiss (Barth et al., 2000; Strickland et al., 2013; Wasserburg et al., 1959) and early Mesoproterozoic porphyritic quartz monzonite (Labotka et al., 1980). The Pahrump Group is a 1.5–4 km thick mixed carbonate and siliciclastic succession that unconformably overlies these basement lithologies (Figure 3; Macdonald et al., 2013; Wright et al., 1974). Formations of the Pahrump Group include the Mesoproterozoic Crystal Spring Formation, the Tonian Horse Thief Springs Formation, the Tonian Beck Spring Dolomite, and the Cryogenian Kingston Peak Formation (Macdonald et al., 2013; Mahon et al., 2014b). A >300 Myr unconformity separates the Crystal Spring Formation, which contains mafic sills, and the overlying Horse Thief Springs Formation, which contains <775.4 ± 0.7 Ma detrital zircon (Dehler et al., 2023; Mahon et al., 2014b; Figure 3) and does not contain the sills. The region experienced Permian-Triassic contraction and magmatism (Snow et al., 1991; Stevens et al., 1997) followed by the Mesozoic Cordilleran orogeny (Burchfiel et al., 1970, 1992; Snow et al., 1991). Neogene felsic and mafic magmatism (Figure 2), high-angle normal faults, basement detachment faults, as well as transform faults associated with extensional tectonism are widespread in the region (Calzia & Rämö, 2000; Renik & Christie-Blick, 2013; Snow, 2000; Wright et al., 1974; Wrucke et al., 2007).

Tilting of crustal blocks related to Neogene extension in Death Valley resulted in the exposure of numerous sills and dikes that intrude the basement rocks and the Crystal Spring Formation. The thickness of the mafic sills ranges from <1 m to over a hundred meters (Hammond, 1983; Wright & Troxel, 1968). Chilled margins against the Crystal Spring Formation have a finer grain size than the sill interiors. Talc deposits up to 30 m thick are developed along contacts between the mafic and the dolomitic lithofacies of the Crystal Spring Formation (Wright & Troxel, 1968). Mining of talc within these contact metamorphosed zones has resulted in striking white scars in the regional landscape next to some of the sills. Olivine, pyroxene and plagioclase are typically altered within the sills (Hammond, 1983). Based on major and trace element data developed from intrusions in multiple localities in Death Valley, Hammond (1986) interpreted that the petrogenesis of the intrusions can be explained by a mantle-derived magmatic source with minimal differentiation and crustal contamination.

Heaman and Grotzinger (1992) developed U-Pb TIMS dates from baddeleyite separated from pegmatitic zones within two mafic sills that outcrop in the southern Ibex Hills near Saratoga Spring in Death Valley National Park and in the Kingston Range (Figure 2a). Due to Pb loss in baddeleyite, the resultant dates are discordant, with interpreted concordia upper intercept ages of 1,069 ± 3 Ma and 1,087 ± 3 Ma (2σ). The sill from Saratoga Spring yielded a lower intercept age of ca. 65 Ma which Heaman and Grotzinger (1992) interpreted to be related to growths of younger zircon rims around older baddeleyite crystals. In addition, Wasserburg et al. (1964) obtained a ca. 235 Ma K-Ar age from a Mesoproterozoic mafic sill in the Crystal Spring Formation that outcrops in Warm Spring Canyon. Although the baddeleyite lower intercept age and the K-Ar age are roughly constrained, these ages are consistent with the mafic sills having been affected by Mesozoic and Cenozoic metamorphism (Snow, 2000; Snow & Wernicke, 1989). Recently, Mohr et al. (2024) extracted zircons from granophyric segregations within two mafic sills from Warm Spring Canyon and one from the central Ibex Range (Figure 2a).

21699356, 2024, 10, Downloaded from https://agupubs.onlinelibrary.wiley.com/doi/10.1029/2024JB029036 by Yiming Zhang - University Of Minnesota Lib, Wiley Online Library on [19/10/2024]. See the Terms and Conditions (https://onlinelibrary.wiley.com/terms-and-conditions) on Wiley Online Library for rules of use; OA articles are governed by the applicable Creative Commons License

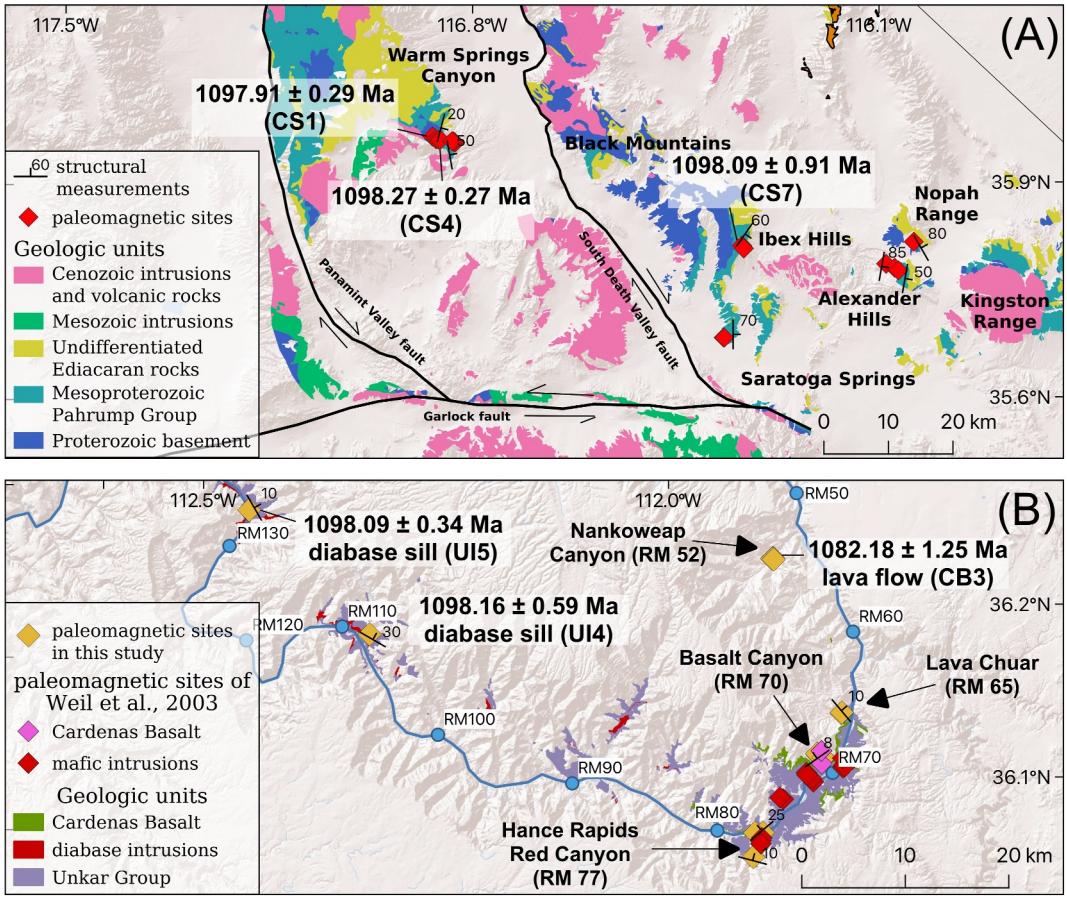

Figure 2. (a) Simplified geologic map of southern Death Valley, CA, (with units modified from Workman et al. (2003) and Wrucke et al. (2007)), showing the location of mafic sills that were sampled for paleomagnetism in this study and geochronology in Mohr et al. (2024). The Mesozoic and Cenozoic intrusions that occur in close proximity to the mafic sills have the potential to have resulted in variable degrees of alteration and magnetic overprints. The mafic sills typically were emplaced parallel to host sedimentary beds in the Crystal Spring Formation, but also intrude older crystalline lithologies. In the field, we collected multiple orientation measurements for sills from contact planes or adjacent sedimentary beds. An average orientation was calculated for each sill and was used to tilt-correct the paleomagnetic data. The representative orientations summarized on the map show that different regions are variably tilted. (b) Simplified geologic map of the Grand Canyon with units modified from Billingsley (2000) and Billingsley and Wellmeyer (2003) showing sedimentary rocks of the Unkar Group, mafic sills and dikes that intruded the sedimentary rocks, and the Cardenas Basalt that is the uppermost unit within the Unkar Group (Figure 3). "RM" stands for river mile using the widely adopted nomenclature for tracking distance through Grand Canyon. Bedding orientations at Nankoweap Canyon were collected from lava flow tops and the bedding of the overlying Nankoweap Formation which have very similar orientations; orientations at Lava Chuar Canyon were collected from the lava flow tops; orientations at Basalt Canyon were collected from lava flow tops, interflow sedimentary rocks, and the Dox Formation stratigraphically below the Cardenas Basalt. These bedding measurements were used for tilt-correcting paleomagnetic data. All geochronology data shown are U-Pb zircon ages from Mohr et al. (2024).

High-precision CA-ID-TIMS zircon U-Pb geochronology yielded indistinguishable $^{206}Pb/^{238}U$ ages of 1,097.91 ± 0.29 Ma, 1,098.27 ± 0.27 Ma, and 1,098.09 ± 0.91 Ma from the three individual sills (95% confidence; Figures 1b, 2a, and 3). These high-precision U-Pb zircon ages, together with previous geochemical data (Hammond, 1986), are consistent with the interpretation that a pulse of ca. 1,098 Ma magmatism led to the emplacement of the mafic intrusions within the Crystal Spring Formation.

2.2. Mafic Intrusions in the Unkar Group

The Grand Canyon Supergroup is divided into the Mesoproterozoic Unkar Group and the Neoproterozoic Chuar Group (Dehler et al., 2017; Elston, 1989; Gundy, 1951). The ~2 km-thick Unkar Group contains the Bass Formation, Hakatai Shale, Shinumo Quartzite, Dox Formation, and Cardenas Basalt (Figure 3; Beus et al., 1974;

21699356, 2024, 10, Downloaded from https://agupubs.onlinelibrary.wiley.com/doi/10.1029/2024JB029036 by Yiming Zhang - University Of Minnesota Lib , Wiley Online Library on [19/10/2024]. See the Terms and Conditions (https://onlinelibrary.wiley.com/terms-and-conditions) on Wiley Online Library for rules of use; OA articles are governed by the applicable Creative Commons License

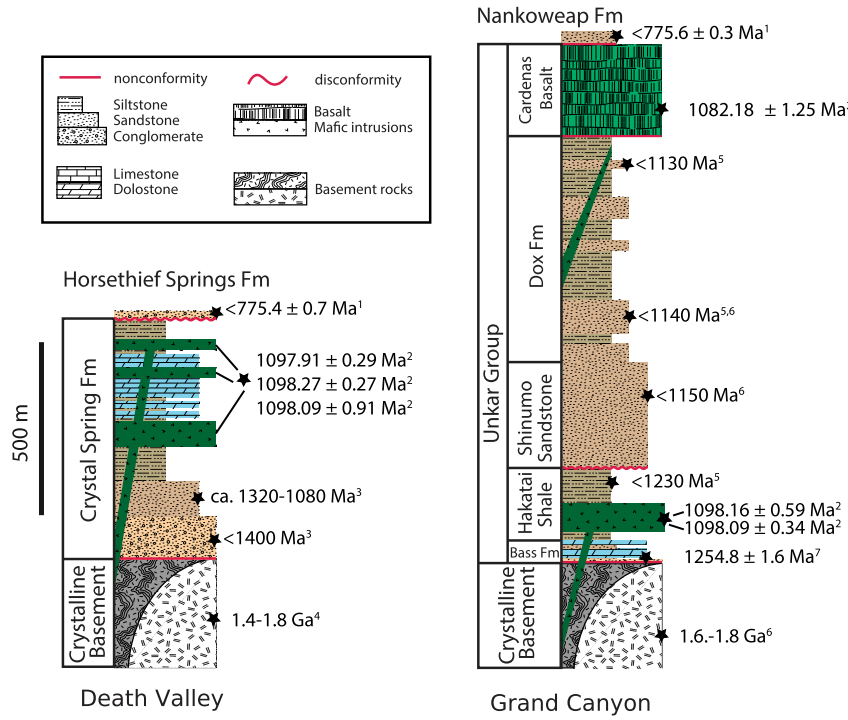

Figure 3. Simplified regional Mesoproterozoic stratigraphy in context of older basement rocks and younger Neoproterozoic sedimentary rocks and compiled geochronology in Death Valley and Grand Canyon. Red lines represent nonconformities and red wavy curves represent disconformities. Black stars are existing radioisotopic age constraints. [1]CA-ID-TIMS U-Pb detrital zircon dates (Dehler et al., 2023); [2] CA-ID-TIMS U-Pb zircon dates (Mohr et al., 2024); [3] LA-MC-ICPMS U-Pb detrital zircon dates (Mahon et al., 2014a); [4] muscovite, biotite, and potassium feldspar ^{40}K-^{40}Ar and ^{87}Rb-^{87}Sr dates (Lanphere, 1964), biotite, muscovite, and hornblende ^{40}Ar-^{39}Ar dates (Labotka et al., 1985), and SHRIMP U-Pb zircon and monazite dates (Barth et al., 2001, 2009); [5] compiled and new detrital zircon and detrital muscovite dates (Mulder et al., 2017); [6] detrital zircon and detrital muscovite dates (Timmons et al., 2005);[7]ID-TIMS U-Pb zircon age from an ash layer (Timmons et al., 2005).

Elston 1989). It is interpreted that the Unkar Group dominantly records shallow marine and fluvial depositional environments (Elston, 1989; Hendricks, 1989; Sears, 1990; Timmons et al., 2005). Siliclastic deposition continued during eruption of the Cardenas Basalt resulting in interflow siltstone and sandstones—commonly with mudcracks and current ripples, respectively (Figure 4). Unkar Group strata typically dip at ~10° to the northeast (Figure 2b) toward normal faults that dip ~60° to the southwest (Sears, 1973; Timmons et al., 2012). Intra-formational faults and large thickness changes in sedimentary units across faults indicate that the Unkar Group was deposited in an extensional tectonic setting (Karlstrom & Humphreys, 1998; Sears, 1990; Timmons et al., 2001).

Numerous mafic sills and dikes intrude the Unkar Group, but not the overlying Chuar Group (Figures 2b and 3; Elston, 1989). Sills typically intrude the Bass Formation and the Hakatai Shale of the lower Unkar Group (Hendricks, 1989) whereas mafic dikes have been mapped that crosscut the Shinumo Sandstone and the Dox Formation of the upper Unkar Group (Timmons et al., 2012). Typical dike plane orientations are subparallel to NW-trending faults in the Unkar Group (Huntoon et al., 1996; Timmons et al., 2012). The sills typically range in thickness between 20 to over 100 m and are (trachy)basalt in composition (Hendricks, 1989; Larson et al., 1994; Figure S1 in Supporting Information S1). Given their spatial proximity and stratigraphic relationship, it had been commonly inferred that all mafic intrusions in the Unkar Group are feeders to the Cardenas Basalt (e.g., Huntoon et al., 1996; Timmons et al., 2012), though no direct feeder relationships have been observed.

The interior of the thick mafic sills are medium-to coarse-grained with subophitic to ophitic texture characterized by plagioclase and olivine grains being enclosed by poikilitic pyroxenes (Hendricks, 1989). The intrusions are fine-grained at their margins where they are chilled against the Unkar sedimentary rocks. Some of the sill interiors

21699356, 2024, 10, Downloaded from https://agupubs.onlinelibrary.wiley.com/doi/10.1029/2024JB029036 by Yiming Zhang - University Of Minnesota Lib , Wiley Online Library on [19/10/2024]. See the Terms and Conditions (https://onlinelibrary.wiley.com/terms-and-conditions) on Wiley Online Library for rules of use; OA articles are governed by the applicable Creative Commons License

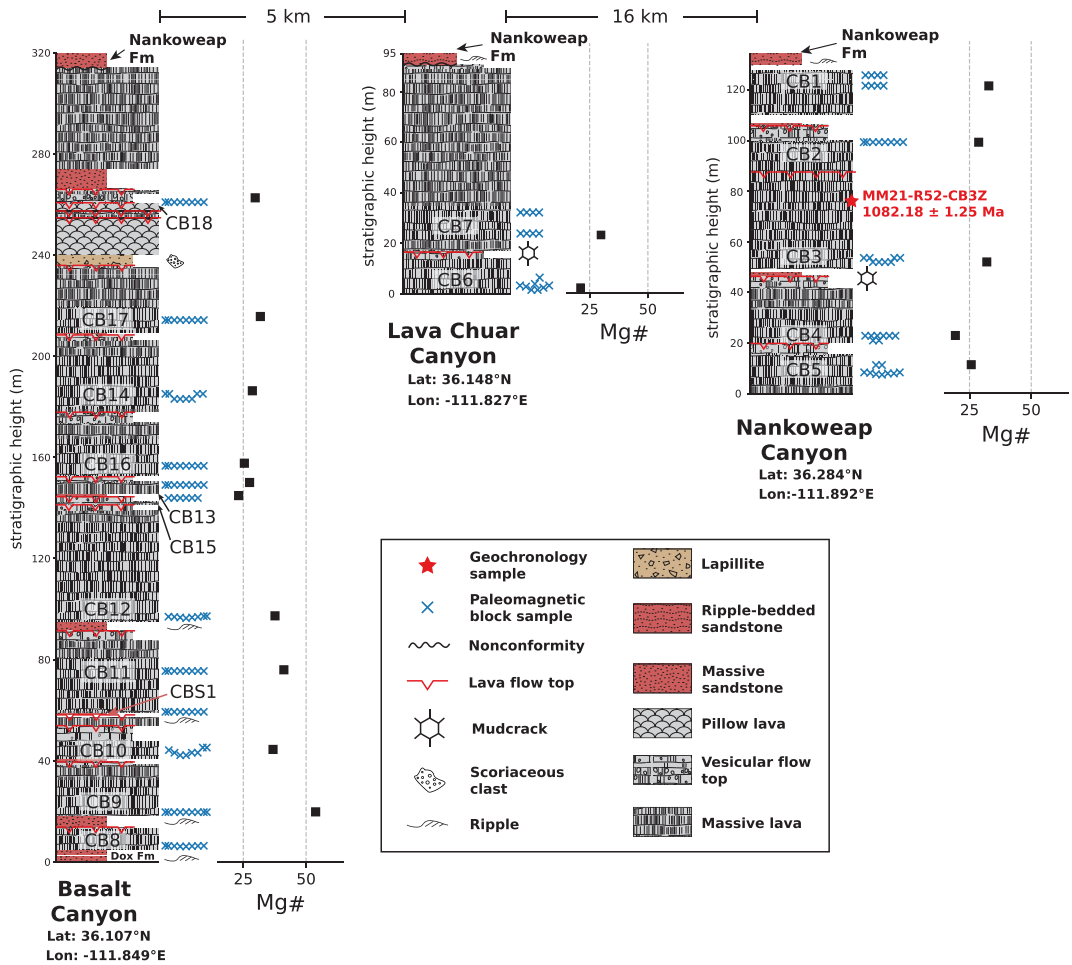

Figure 4. Volcanostratigraphy of the Cardenas Basalt at Basalt Canyon, Lava Chuar Canyon, and Nankoweap Canyon measured in this study. Section locations are shown in Figure 2b. Stratigraphic locations of the collected paleomagnetic samples and the geochronology sample dated by Mohr et al. (2024) are shown. The Mg# values calculated as $\frac{MgO}{MgO+FeO} \times 100$ based on the major element XRF data developed in this study are plotted against the sample stratigraphic levels. The major element geochemistry data can be found in Table S1 in Supporting Information S1. The interflow sandstones and vesicular lava flow tops distinguish individual lava flows such that paleomagnetic samples from each lava flow constitute a site (labeled as "CB" with distinct numbers). The latitude and longitude values correspond to the base of the stratigraphic sections.

contain zircon-bearing segregations (Mohr et al., 2024), which were dated with high-precision CA-ID-TIMS $^{206}Pb/^{238}U$ at 1,098.16 ± 0.59 Ma at Hotauta Canyon (river mile [RM] 107) and 1,098.09 ± 0.34 Ma at Stone Creek (RM 132) (Figures 1b and 2b; 95% confidence).

2.3. Cardenas Basalt

The Cardenas Basalt at the top of the Unkar Group exclusively outcrops in eastern Grand Canyon (Figure 2b). The most complete section of the Cardenas Basalt outcrops in the Basalt Canyon area where ~315 m of stratigraphy including lava flows and associated interflow sedimentary rocks are preserved up to the unconformity between the volcanics and the overlying Nankoweap Formation (Figures 2b and 4; Hendricks, 1989; Lucchitta & Hendricks, 1983). Cardenas Basalt also outcrops with variable thicknesses at localities including Lava Chuar Canyon and Nankoweap Canyon (Figures 2b and 4). The lava flows are typically (trachy)basaltic andesite in composition, overall having higher SiO_2 values than the mafic intrusions in the Unkar Group (Figure S1 in Supporting Information S1; Hendricks, 1989; Larson et al., 1994).

Previous studies constructed volcanostratigraphic sections of the Cardenas Basalt at Basalt Cliffs, Ochoa Point, Basalt Canyon, and Lava Chuar Canyon (Hendricks, 1989; Lucchitta & Hendricks, 1983). In particular,

21699356, 2024, 10, Downloaded from https://agupubs.onlinelibrary.wiley.com/doi/10.1029/2024JB029036 by Yiming Zhang - University Of Minnesota Lib , Wiley Online Library on [19/10/2024]. See the Terms and Conditions (https://onlinelibrary.wiley.com/terms-and-conditions) on Wiley Online Library for rules of use; OA articles are governed by the applicable Creative Commons License

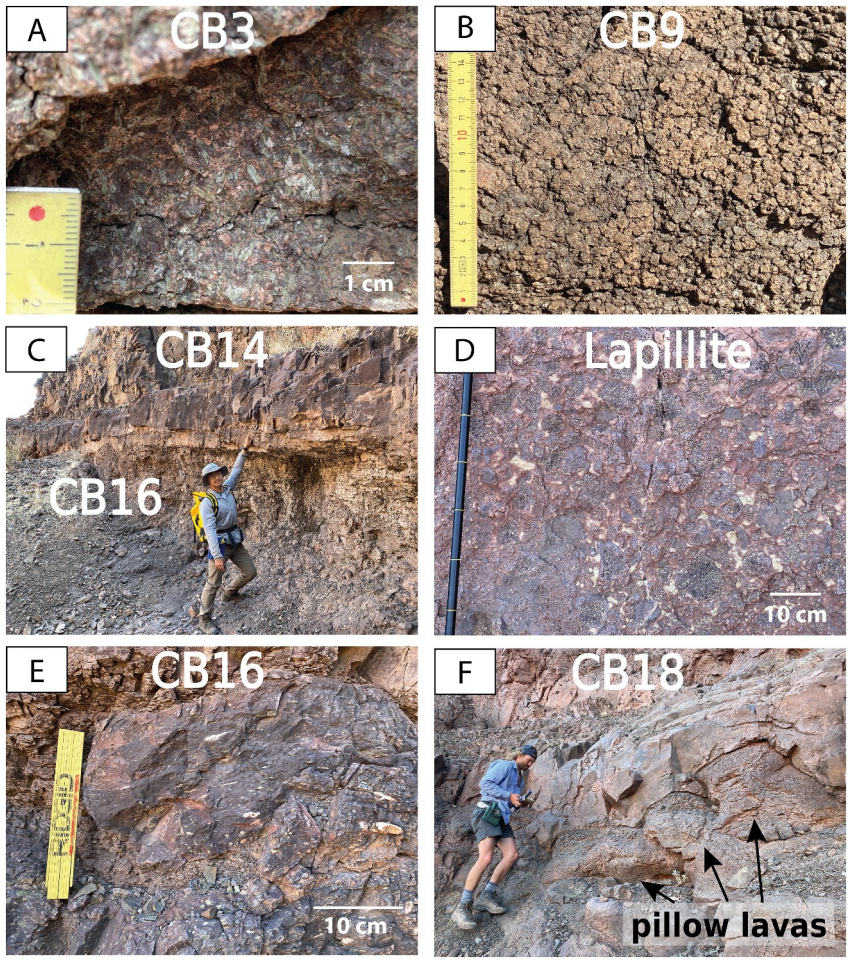

Figure 5. Field photos of Cardenas Basalt. The site names correspond to those shown in the stratigraphic section in Figure 4. (a) Coarse-grained interior of the 57 m thick CB3 lava flow at Nankoweap Canyon (Figure 4) from which zircon were extracted and dated by Mohr et al. (2024). (b) Ophitic texture in the interior of flow CB9 at Basalt Canyon. Individual oikocrysts reach diameters of 9 mm. (c) Contact between two individual lava flows CB14 and CB16 (meter level 178 in Figure 4). The massive flow bottom of the upper flow is more resistant to weathering than the recessive vesiculated flow top of the underlying flow leading to the overhang visible in the photograph. (d) The volcaniclastic marker bed containing scoriaceous volcanic clasts surrounded by tan-colored, very fine-grained matrix at 236–240 m in the Basalt Canyon section. (e) Amygdaloidal flow top of CB16. Elongate amygdules indicate that vesicles were stretched during flow. (f) Pillow lavas near the top of the exposed stratigraphy at Basalt Canyon (within interval from meter level 240 to 257; Figure 4).

Hendricks (1989) developed a stratigraphic section at Basalt Canyon with detailed petrologic and lithologic descriptions. In this study, we investigated three sections at Basalt Canyon, Lava Chuar Canyon, and Nankoweap Canyon (Figure 2). We measured volcanostratigraphic sections with a particular focus on determining individual lava flows that represent distinct cooling units such that paleomagnetic samples collected from a single lava flow are considered to capture the same snapshot of the geomagnetic field as they cooled (i.e., a paleomagnetic site; Figure 4). Flow boundaries can be delineated by progressive changes in vesiculation and by highly vesiculated flow tops that are sometimes overlain by interflow clastic sedimentary rocks (Figures 4 and 5e).

At Basalt Canyon, flows in the initial 95 m above the Dox Formation are subophitic to ophitic in texture and heavily weathered with a brownish-green color (Figure 5b). These flows form slopes characterized by small weathered basalt fragments that often are dislodged pyroxene oikocrysts. Walking on steep slopes mantled by these oikocrysts is like walking on ball bearings. Walcott (1883) and Lucchitta (1979) noted that these flows experienced spilitic alteration, interpreted as the result of subaqueous eruptions in a tidal flat or deltaic environment. The claim has also been made that there are pillows in these lower flows (Hendricks et al., 1974; Stevenson & Beus, 1982). However, our field observations, as well as those of Larson et al. (1994) and Elston and

21699356, 2024, 10, Downloaded from https://agupubs.onlinelibrary.wiley.com/doi/10.1029/2024JB029036 by Yinning Zhang - University Of Minnesota Lib , Wiley Online Library on [19/10/2024]. See the Terms and Conditions (https://onlinelibrary.wiley.com/terms-and-conditions) on Wiley Online Library for rules of use; OA articles are governed by the applicable Creative Commons License

Scott (1976), did not find evidence of pillow lava indicative of subaqueous eruptions in these flows. Note that spheroidal weathering can often be misidentified as pillows. While spheroidal weathering, granular grus piles, and ophitic textures on the weathered exposures are common, the features in these basal ophitic flows, including the presence of an observed pahoehoe flow top and basal pipe vesicles, are consistent with them being subaerially erupted sheet flows (Figure 5). A ropy flow top consistent with pahoehoe lava flows was also reported in Hendricks (1989). The upper 200 m of Cardenas Basalt flows consist of more competent, cliff-forming lava flows that are finer-grained than the lower sequence. A 4-m-thick volcaniclastic layer containing cobble-to boulder-sized scoriaceous volcanic clasts surrounded by tan-colored, fine-grained matrix occurs at stratigraphic height of ∼240 m (Figures 4 and 5d). Lucchitta and Hendricks (1983) named this unit the lapillite member of the Cardenas Basalt and interpreted that it likely formed as pyroclastic debris deposited by lahars. Pillow lavas typically 0.8–1 m wide with horizons of volcaniclastic materials consistent with subaqueous eruption are found near the top of the section, above the lapillite layer (Figure 5f).

Shorter sections of Cardenas Basalt flows are exposed in Nankoweap Canyon (RM 52) and Lava Chuar Canyon (RM 65) (Figures 2b and 4). Due to the less complete exposures at these two localities, the volcanostratigraphic correlations between the three localities cannot be unequivocally drawn. The exposure of the unconformity with the overlying Nankoweap Formation at Lava Chuar Canyon and Nankoweap Canyon suggest that flows in those successions could correlate with the upper lavas at Basalt Canyon (Figure 4). The geochemistry of the lavas supports such a correlation as the Mg# of the upper lava flows is distinct from that of the lower ophitic flows as shown in Figure 4. Large lateral variability of individual lava flow thicknesses has been reported (Lucchitta & Hendricks, 1983), indicating that lava flows likely pinch out laterally between the localities. Our stratigraphic sections at the three localities also show variable lava flow thicknesses directly below the Nankoweap Formation (Figure 4) although this could reflect variability in erosional truncation. We treat the sampled lava flows at different localities as distinct cooling units in this study with each being an individual paleomagnetic site (Figure 4). The Mohr et al. (2024) geochronology sample for the Cardenas Basalts comes from the interior of a 57 m thick lava flow at Nankoweap Canyon (Figures 4 and 5a; CB3). Four zircon microlites from this flow yielded a weighted mean $^{206}Pb/^{238}U$ ages of 1,082.18 ± 1.25 Ma (95% confidence; Figure 1b).

3. Methods

A total of 123 samples from 15 individual mafic sills were collected from the Death Valley region (Figure 2a). Core samples were collected with a gasoline-powered drill outside of Death Valley National Park and block samples were collected from sills inside the park. In the Grand Canyon, a total of 184 block samples were collected from 18 individual Cardenas Basalt lava flows, one baked interflow sedimentary bed, and 5 mafic intrusions within the Unkar Group. When sampling, we preferentially targeted the finer-grained margins of flows and intrusions over the coarser-grained interiors. Typically, 6 to 9 samples were collected at each site. Both magnetic compass and sun compass were used when orienting the drill cores and block samples in the field. Sun compass orientations were preferentially used when available. In the lab, standard paleomagnetic cores were drilled from the block samples and then oriented relative to the oriented surfaces.

The locations of the paleomagnetic sites are shown in Figure 2 and Table 1, and the stratigraphic positions of block samples collected from the Cardenas Basalt are shown in Figure 4. Within Warm Spring Canyon in the Death Valley region, we sampled the 1,097.91 ± 0.29 Ma sill as CS1 and the 1,098.27 ± 0.27 Ma sill as CS4, and in Ibex Hills, we sampled the 1,098.09 ± 0.91 Ma sill as CS7 (Figure 2b). Other undated sills are labeled in Figure 2b and locations for all sites are available in the archived data repository (Zhang et al., 2024a). In western Grand Canyon, we sampled the 1,098.16 ± 0.59 Ma sill in Hotauta Canyon as UI4 (RM 107) and the 1,098.09 ± 0.34 Ma Stone Creek Canyon sill as UI5 (RM 132). In the eastern canyon, we sampled the Hance dike north to the Hance Rapids (UI2; RM 77) and the Hance sill south to the rapids (UI3). Another undated mafic sill was sampled at Red Canyon (RM 77) which is south of the river at Hance Rapids along the tributary stream channel of Red Canyon (UI1; Figure 2b).

A suite of specimens from sills in the Crystal Spring Formation underwent step-wise thermal demagnetization up to 680°C. An additional suite of sister specimens from some samples also underwent thermal demagnetization with an added step of a liquid nitrogen bath following the measurement of natural remanent magnetization. This demagnetization step can preferentially remove overprint magnetization held by multidomain titanomagnetite grains and potentially improve the resolution of the characteristic component. All specimens from the Cardenas

21699356, 2024, 10, Downloaded from https://agupubs.onlinelibrary.wiley.com/doi/10.1029/2024JB029036 by Yiming Zhang - University Of Minnesota Lib , Wiley Online Library on [19/10/2024]. See the Terms and Conditions (https://onlinelibrary.wiley.com/terms-and-conditions) on Wiley Online Library for rules of use; OA articles are governed by the applicable Creative Commons License

Table 1
Site-Level Paleomagnetic Data From Mafic Sills in Death Valley, Cardenas Basalt, and Mafic Intrusions in the Unkar Group.

Site	Study region	Geologic type	Site latitude (°N)	Site longitude (°E)	n	dec_{gc}	inc_{gc}	dec_{tc}	inc_{tc}	k	α_{95} (°)	vgp lat (°N)	vgp lon (°E)
CS1[a]	Death Valley	Sill	35.9688	−116.9190	8	303.0	50.0	292.8	73.3	175	4.2	41.7	203.7
CS2	Death Valley	Sill	35.9651	−116.9130	7	290.2	43.2	296.3	65.3	27	11.9	42.5	187.7
CS6	Death Valley	Sill	35.9618	−116.8829	8	275.5	−4.7	281.3	48.4	45	8.3	25.2	172.3
CS7[a]	Death Valley	Sill	35.8154	−116.3886	2	318.0	−8.0	331.1	42.4	167	19.5	62.7	137.2
CS8	Death Valley	Sill	35.8114	−116.3854	9	305.2	5.2	297.1	58.7	78	5.9	41.1	177.8
CS9	Death Valley	Sill	35.8112	−116.3855	5	316.0	−2.0	317.5	52.6	39	12.3	55.1	161.9
CS12	Death Valley	Sill	35.7789	−116.1206	8	284.7	2.3	301.6	63.3	30	10.2	45.5	184.3
CS13	Death Valley	Sill	35.8187	−116.0938	3	269.0	−13.7	293.6	51.2	150	10.1	35.8	170.3
CB1	Grand Canyon	Lava flow	36.2839	−111.8919	8	249.3	52.9	270.3	51.1	200	3.9	18.4	184.5
CB2	Grand Canyon	Lava flow	36.2836	−111.8919	8	276.3	56.5	283.3	78.7	329	3.1	38.2	220.8
CB3[a]	Grand Canyon	Lava flow	36.2833	−111.8928	7	261.3	58.7	249.3	52.9	56	8.1	5.1	196.5
CB4	Grand Canyon	Lava flow	36.2831	−111.8928	7	248.6	35.0	261.3	58.7	37.1	10.0	16.9	196.9
CB5	Grand Canyon	Lava flow	36.2825	−111.8914	9	241.6	45.7	276.3	56.5	71	6.2	25.3	186.8
CB6	Grand Canyon	Lava flow	36.1458	−111.8275	8	270.3	51.1	252.7	47.0	88	5.9	3.8	190.7
CB7	Grand Canyon	Lava flow	36.1464	−111.8269	8	283.3	78.7	269.9	42.5	106	5.4	14.1	178.5
CB8	Grand Canyon	Lava flow	36.1072	−111.8486	8	271.9	53.0	272.7	38.5	132	4.8	14.7	174.5
CB9	Grand Canyon	Lava flow	36.1073	−111.8493	8	264.6	37.4	283.6	27.3	96	5.7	19.3	162.3
CB10	Grand Canyon	Lava flow	36.1075	−111.8489	7	264.0	32.3	273.9	38.0	88	6.5	15.4	173.6
CB11 & CBS1	Grand Canyon	Lava flow: Sediments	36.1082	−111.8489	13	278.1	28.4	268.3	69.5	93.2	4.3	27.2	206.5
CB12	Grand Canyon	Lava flow	36.1100	−111.8531	8	265.9	37.1	268.8	42.0	193	4.0	13.1	178.8
CB13	Grand Canyon	Lava flow	36.1101	−111.8542	7	259.9	40.0	267.0	6.1	107	5.9	−0.6	162.4
CB14	Grand Canyon	Lava flow	36.1108	−111.8553	7	266.0	4.6	259.4	52.9	514	2.7	11.6	191.3
CB15	Grand Canyon	Lava flow	36.1103	−111.8533	6	247.4	49.1	263.3	45.7	89	7.1	10.7	184.1
CB16	Grand Canyon	Lava flow	36.1100	−111.8547	7	253.6	42.8	266.2	17.5	63	7.7	2.2	167.6
CB17	Grand Canyon	Lava flow	36.1114	−111.8553	8	263.2	15.7	264.8	49.3	253	3.5	13.5	185.9
CB18	Grand Canyon	Lava flow	36.1117	−111.8558	7	253.6	46.5	285.6	52.3	98	6.1	30.2	178.9
UI1	Grand Canyon	Sill	36.0247	−111.9300	8	243.9	66.1	269.1	23.9	216	3.8	6.6	168.7
UI2	Grand Canyon	Dike	36.0456	−111.9183	8	263.9	19.3	264.0	10.0	75	6.5	−1.9	165.7

21699356, 2024, 10, Downloaded from https://agupubs.onlinelibrary.wiley.com/doi/10.1029/2024JB029036 by Yiming Zhang - University Of Minnesota Lib , Wiley Online Library on [19/10/2024]. See the Terms and Conditions (https://onlinelibrary.wiley.com/terms-and-conditions) on Wiley Online Library for rules of use; OA articles are governed by the applicable Creative Commons License

Table 1
Continued

Site	Study region	Geologic type	Site latitude (°N)	Site longitude (°E)	n	dec_{gc}	inc_{gc}	dec_{tc}	inc_{tc}	k	α_{95} (°)	vgp lat (°N)	vgp lon (°E)
UI3	Grand Canyon	Sill	36.0458	−111.9267	8	258.1	20.4	264.1	25.6	139	4.7	3.2	172.4
U14[a]	Grand Canyon	Sill	36.2353	−112.3294	7	264.0	14.3	314.1	51.6	54	8.3	52.2	165.4
U15[a]	Grand Canyon	Sill	36.3483	−112.4525	8	278.2	49.2	295.6	49.3	76	6.4	36.8	170.8

Note. *n* represents the number of samples used for calculating site mean statistics. dec_{gc} and inc_{gc} are site mean declination and inclination in geographic coordinates. dec_{tc} and inc_{tc} are site mean declination and inclination in tilt-corrected coordinates. k represents the Fisher concentration parameter of the site level mean directions in tilt-corrected coordinates. α_{95}° represents the Fisher 95% angular uncertainty of the site level mean directions in tilt-corrected coordinates. *vgp lat* and *vgp lon* represent the latitude and longitude of the site-level virtual geomagnetic poles calculated from tilt-corrected directional data. [a]marks sites that have paired high-precision zircon U-Pb ages developed by Mohr et al. (2024). CS1 is dated to be 1,097.91 ± 0.29 Ma; CS7 is dated to be 1,098.09 ± 0.91 Ma; CB3 is dated to be 1,082.18 ± 1.25 Ma; UI4 is dated to be 1,098.16 ± 0.59 Ma; UI5 is dated to be 1,098.09 ± 0.34 Ma. All ages are presented with 95% confidence.

Basalt and the mafic intrusions within the Unkar Group underwent step-wise thermal demagnetization up to 580°C with some samples continuing up to 680°C. The thermal demagnetization protocol had increasingly higher resolution approaching the Curie temperature of magnetite (~580°C) and Néel temperature of hematite (~680°C).

All demagnetization experiments were carried out in the magnetically shielded room at the UC Berkeley Paleomagnetism Lab. The typical magnetic field inside the shielded room is <500 nT. An ASC TD-48SC thermal demagnetizer with <10 nT field inside the chamber was used for the demagnetization steps. All remanence measurements were made on a 2G Enterprises DC-SQUID superconducting rock magnetometer. The PmagPy software package (Tauxe et al., 2016) was used to implement least-square fits (Kirschvink, 1980) to specimen demagnetization data.

In the Death Valley region, multiple bedding orientations were measured along contacts between the sills and the host sedimentary rocks and along bedding of sedimentary rocks near the sills, and the averages of these measurements were used to tilt-correct paleomagnetic directions of each sill. In the Grand Canyon, the contact planes between the Hance sill and the adjacent sedimentary layers are poorly exposed. We collected bedding measurements from the nearby exposures of the Bass Formation for tilt correction. We also collected orientations from the Hance sill columnar joint planes—planes that are typically vertical prior to tilting. The best-fit plane orthogonal to the columnar joint planes has an orientation similar to the mean bedding plane of the Bass Formation (Figure S3 in Supporting Information S1). We use the mean bedding plane of the Bass Formation for tilt correction. Bedding orientations of the host Hakatai Shale were used to tilt-correct the Hance dike paleomagnetic data. Bedding orientations were taken on the Cardenas Basalt flow tops and on interflow sediments for tilt correction. All bedding orientation data are available in the archived data repository (Zhang et al., 2024a).

We also acquired new whole-rock major and trace element geochemistry data from the 18 Cardenas Basalt lava flows and the 5 mafic intrusions in the Grand Canyon. The data were developed at the WSU GeoAnalytical Lab. The details of the experimental method and precision can be found at https://environment.wsu.edu/facilities/geoanalytical-lab/technical-notes/. All data can be accessed at Zhang et al. (2024a).

4. Results and Interpretations

Eight out of the 15 mafic sills from the Death Valley area yielded stable, consistent, and interpretable paleomagnetic directional data. In the Grand Canyon, all sites including 5 mafic sills, 18 lava flows, and one interflow sedimentary bed yielded well-grouped, consistent paleomagnetic directions. The site-level paleomagnetic statistics are summarized in Table 1. Data to the individual measurement level are available in the MagIC database (https://doi.org/10.7288/V4/MAGIC/20009).

21699356, 2024, 10, Downloaded from https://agupubs.onlinelibrary.wiley.com/doi/10.1029/2024JB029036 by Yiming Zhang - University Of Minnesota Lib, Wiley Online Library on [19/10/2024]. See the Terms and Conditions (https://onlinelibrary.wiley.com/terms-and-conditions) on Wiley Online Library for rules of use; OA articles are governed by the applicable Creative Commons License

4.1. Death Valley Region Mafic Sills

Thermal demagnetization results on specimens with stable and consistent remanence from the Death Valley sills show that the specimens typically have an overprint component (Figure 6). That component can be removed by heating up to ~500°C, although it is largely removed after heating to 100°C in most specimens. The liquid nitrogen demagnetization step (77 K) was also efficient in removing this component. Following the removal of this low-temperature component, an origin-trending component was resolved through progressive thermal demagnetization steps up to the Curie temperature of magnetite (i.e., ~580°C; Figure 6). This behavior is consistent with low-titanium titanomagnetite carrying the characteristic remanence in these rocks. For sites CS7 and CS13 (Table 1), the characteristic component and the secondary overprint component have wide ranges of overlapping unblocking temperatures such that the characteristic component is not well-isolated in some specimens. As a result, only two specimens in CS7 and three specimens in CS13 yielded well-defined characteristic remanence directions. The other sills failed to yield high-fidelity site-level directional results. Specimens from those sills often show inconsistent thermal demagnetization behaviors, have weak natural remanent magnetizations that become unstable at high temperatures, or have secondary remanence components with unblocking temperature ranges that significantly overlap with those of the characteristic remanence component such that the characteristic components cannot be well-fitted by a straight least-squares line. These non-ideal behaviors are likely due to alteration of primary ferromagnetic minerals associated with hydrothermal fluids during emplacement of the sills (Hammond, 1983, 1986), or heating and alteration associated with Mesozoic and Cenozoic magmatism in the region (Snow & Wernicke, 1989; Snow, 2000; Figure 2a).

In geographic coordinates, the site level low-temperature component directions of the Death Valley sills lie very close to the direction of the present-day geomagnetic field direction in Death Valley (Figure 7). The low unblocking temperature and the directions of this component are consistent with it being a geologically recent viscous remanence overprint (Moskowitz et al., 1998; Muxworthy & McClelland, 2000). On the other hand, the origin-trending component in the sills removed at higher temperatures is directed to the northwest with steep downward inclinations after tilt correction (purple mid-temperature component in Figures 6 and 7). Eight sills yielded consistent results within site and well-grouped mean directions amongst sites. Figure 8a shows the virtual geomagnetic poles (VGPs) and the mean pole position (pole longitude = 176.6°E, pole latitude = 44.9°N, $N = 8$, $A_{95} = 11.8°$; no rotation correction) calculated from the tilt-corrected sills in Death Valley. This pole position passes the paleosecular test of Deenen et al. (2011) as its A_{95} of 11.8° passes the criterion of being between 5.2° and 22.1° for this number of sites.

4.2. Grand Canyon Unkar Group Intrusions and Cardenas Basalt

The two dated ca. 1,098 Ma sills in eastern Grand Canyon (UI4 and UI5) and three intrusions near Hance Rapids and in Red Canyon (UI1, UI2, and UI3; Figure 2b) all yielded consistent within-site thermal demagnetization results and have similar thermal demagnetization behaviors between sites (Figures 6 and 7). Typically, an origin-trending characteristic remanence component unblocks between 500°C and 585°C after a secondary overprint component that overlaps with the present local field direction is removed at lower temperatures (Figure 6). This thermal demagnetization behavior indicates that the characteristic remanence components in these mafic intrusions are held by low-titanium titanomagnetite. Despite their similar demagnetization behaviors, the mafic intrusions record two distinct groups of remanence directions (Figure 7). The ca. 1,098 Ma mafic sills in Hotauta Canyon (UI4) and Stone Creek Canyon (UI5) record paleomagnetic directions to the northwest with steep inclinations, whereas the other three undated intrusions in eastern Grand Canyon have westerly directions and much shallower inclinations (Figures 6 and 7).

Thermal demagnetization of the 18 Cardenas Basalt lava flows yielded consistent site-level results (Figure 7). After an overprint component that overlaps with the present local field direction was removed by heating up to 300°C (Figure 6), the specimens typically demagnetized along an origin-trending path approaching 580°C. Some specimens continued to demagnetize up to the Néel temperature of hematite (~690°C; Özdemir & Dunlop, 2006; Figure 6). The unblocking temperature ranges indicate that titanomagnetite and hematite are the dominant remanence-carrying minerals in the lava flows. Least-squares line fits made for the magnetite and hematite components have very similar directions in the same specimens (Figure 6; CB1-1a). This result is consistent with the hematite having formed due to early oxidation of the lava flows and acquired remanent magnetization soon after the eruption of the lavas.

21699356, 2024, 10, Downloaded from https://agupubs.onlinelibrary.wiley.com/doi/10.1029/2024JB029036 by Yiming Zhang - University Of Minnesota Lib , Wiley Online Library on [19/10/2024]. See the Terms and Conditions (https://onlinelibrary.wiley.com/terms-and-conditions) on Wiley Online Library for rules of use; OA articles are governed by the applicable Creative Commons License

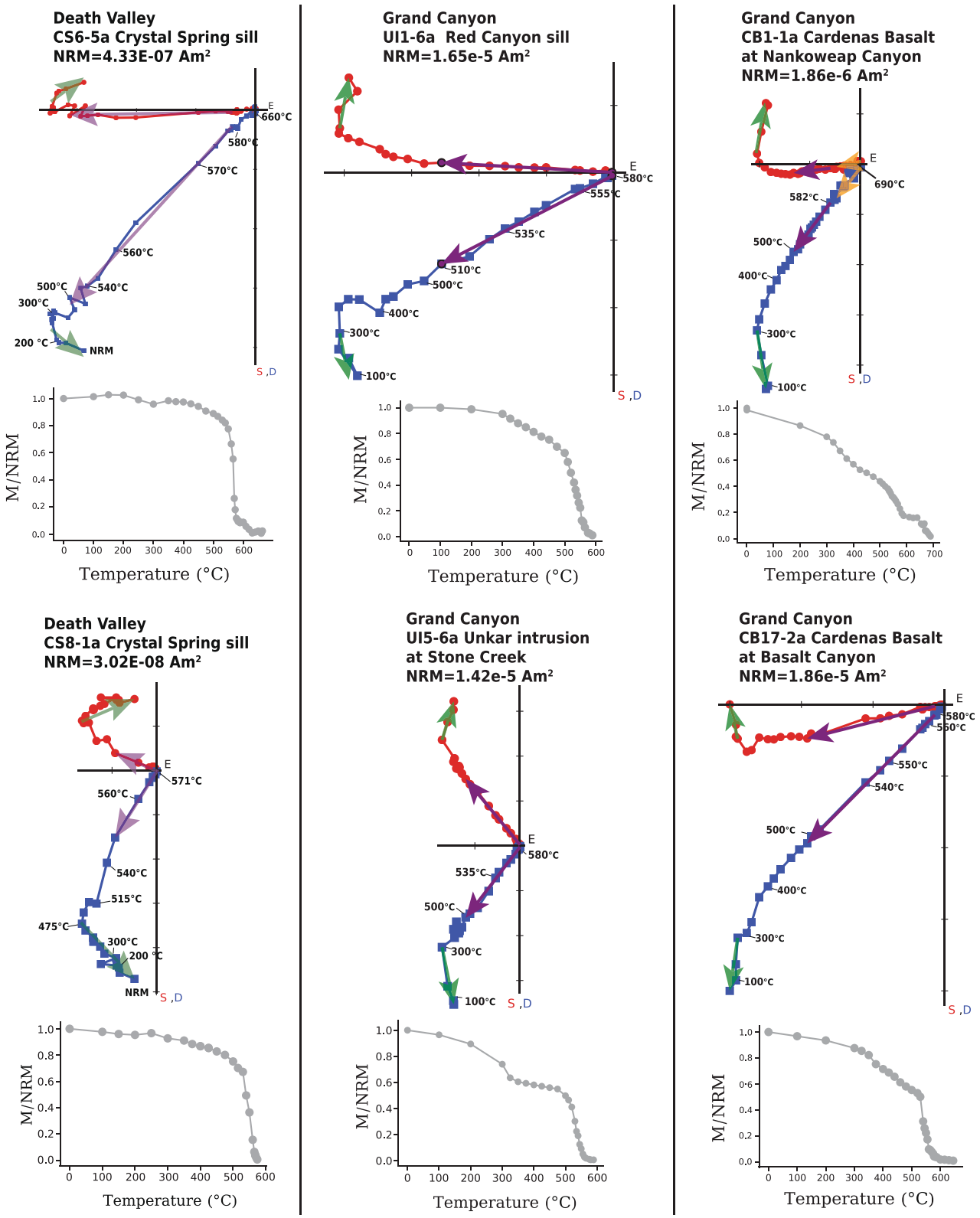

Figure 6.

21699356, 2024, 10, Downloaded from https://agupubs.onlinelibrary.wiley.com/doi/10.1029/2024JB029036 by Yiming Zhang - University Of Minnesota Lib , Wiley Online Library on [19/10/2024]. See the Terms and Conditions (https://onlinelibrary.wiley.com/terms-and-conditions) on Wiley Online Library for rules of use; OA articles are governed by the applicable Creative Commons License

21699356, 2024, 10, Downloaded from https://agupubs.onlinelibrary.wiley.com/doi/10.1029/2024JB029036 by Yiming Zhang - University Of Minnesota Lib , Wiley Online Library on [19/10/2024]. See the Terms and Conditions (https://onlinelibrary.wiley.com/terms-and-conditions) on Wiley Online Library for rules of use; OA articles are governed by the applicable Creative Commons License

Site-level characteristic directions for all of the intrusions in Grand Canyon as well as Cardenas Basalt flows except for CB4 were calculated using the (titano)magnetite-bearing components. This component is referred to as the "mid-temperature direction" in Figure 7. For site CB4, all except for one specimen have antipodal components, both of which we interpret to be carried by hematite. The antipodal directions recorded within the same specimens may be the result of magnetic self-reversal associated with the oxidation of magnetite into maghemite which subsequently inverted into hematite (Swanson-Hysell et al., 2011). A detailed description of the specimen results for site CB4 is presented in Figure S4 in Supporting Information S1. We combine the normal-polarity (i.e., directions pointing southwest and down) directions held by hematite in six samples together with a normal polarity direction carried by titanomagnetite in one sample for calculating a site mean direction for this flow. Seven samples collected from a baked interflow red sandstone layer (site CBS1) within 0.2 m of the base of lava flow CB11 yielded overlapping paleomagnetic directions with those from the overlying lava flow (Figure S5 in Supporting Information S1). We group the samples from the lava flow and the baked sediments as one site when calculating the mean direction and VGP.

The major and trace element geochemistry data for the Cardenas Basalt and the mafic Unkar intrusions are presented in Tables S1 and S2 in Supporting Information S1. The total alkali-silica diagram and chondrite-normalized rare earth element diagram for the lava flows and intrusions based on the new data together with previously developed data (Hendricks, 1989; Larson et al., 1994) are shown in Figures S1 and S2 in Supporting Information S1. Figure 4 shows the Mg values (labeled as Mg# on the horizontal axis) plotted against sample stratigraphic heights for the Cardenas Basalt lava flows. The Mg# values are calculated based on the normalized XRF major element geochemistry data (Table S1 in Supporting Information S1). That the basal flows at Basalt Canyon have higher Mg# values than the upper flows indicate that the section captured a geochemical evolution of the Cardenas Basalt where it was less primitive later in the eruptive history.

Figure 8b shows the VGPs of the two dated ca. 1,098 Ma sills in eastern Grand Canyon (UI4 and UI5) and the VGPs of the intrusions near Hance Rapids and Red Canyon (UI1, UI2, and UI3) from this study. The mean pole position for the Cardenas Basalt is plotted with the VGPs in Figure 9 (pole longitude = 183.9°E, pole latitude = 15.9°N, $N = 18$, $A_{95} = 7.4°$, $K = 22.7$; no rotation correction). The Cardenas Basalt pole passes the secular variation test of Deenen et al. (2011) as its A_{95} of 7.4° passes the criterion of being between 3.8° and 13.3° for this number of sites.

5. Discussion

5.1. Origin of Characteristic Remanence of Mafic Intrusions and the Cardenas Basalt in Southwestern Laurentia

The Death Valley mafic sills that we sampled belong to range-scale crustal blocks that were rotated by various amounts during the Neogene. These blocks include the Panamint Mountains, the Black Mountains, and the Nopah Range (Figure 2a). Sedimentary strata in the Crystal Spring Formation in these blocks dip variably to the east (Figure 2a). The mafic sills intruded parallel to the bedding of the Crystal Spring Formation, often taking advantage of contacts between different lithologies such as the contact between the argillite facies and the cherty dolomite facies. The dips of the sills vary between ~23° to ~86°. The characteristic paleomagnetic remanence directions from the sills in the blocks are much better grouped when corrected for this tilt (dec = 302.8°, inc = 58.0°, $n = 8$, $A_{95} = 9.5°$, $k = 34.8$) than when considered in geographic coordinates without tilt correction (dec = 295.1°, inc = 8.9°, $A_{95} = 21.6°$, $k = 7.5$; Figure S6 in Supporting Information S1). This result is consistent with the interpretation that the characteristic remanence component carried by (titano)magnetite in the sills is a primary remanence acquired during initial cooling prior to tilting of the Crystal Spring Formation.

Figure 6. Example orthogonal vector diagrams of specimen thermal demagnetization results from mafic sills that intruded the Crystal Spring Formation, mafic sills that intruded the Unkar Group, and the Cardenas Basalt. Total specimen magnetic moments (M) normalized by the natural remanent magnetizations (NRM) are plotted against temperature steps. The low-temperature component (green) in the rocks can be removed by heating typically to ~300°C, but can be up to ~500°C. It corresponds to the present local field direction (Figure 7) and is interpreted as an overprint. The mid-temperature component (purple) is origin-trending and typically unblocks sharply through ~500–580°C, consistent with a primary thermal remanent magnetization held by titanomagnetite. In some Cardenas lava flows such as CB1, a third high-temperature component unblocks up to ~690°C, and is interpreted to be carried by hematite that formed during early oxidation. All orthogonal plots are shown in tilt-corrected coordinates.

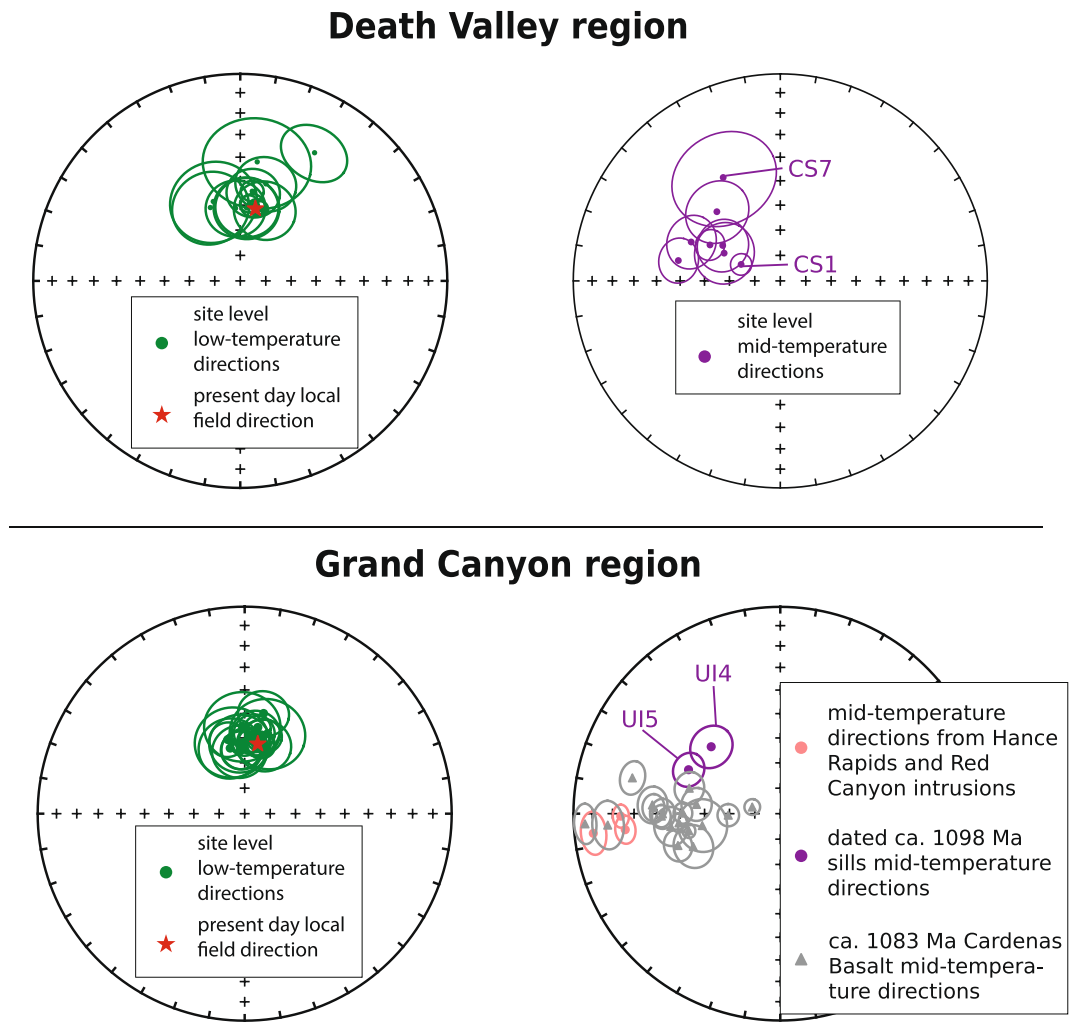

Figure 7. Summary equal area diagrams for the site level directional results from the Death Valley region and the Grand Canyon region. The site level low-temperature components (green) in geographic coordinates are shown in context of present-day local field directions (red star) at the study localities. The mid-temperature directions (i.e., those that unblock over a temperature range consistent with titanomagnetite) are shown in tilt-corrected coordinates. Note that the directions from the mafic sills at Hotauta Canyon (UI4) and Stone Creek (UI5) (directions shown in purple) are more northerly and steeper than the directions of many Cardenas lava flows and the intrusions near Hance Rapids (shown in gray and pink).

The new paleomagnetic pole from the Cardenas Basalt does not have an associated field test. The flows are all of normal polarity as expected for their age given that they erupted during the ca. 1,099 to <1,075 Ma Portage Lake normal polarity zone (Swanson-Hysell et al., 2019), which is interpreted to be a superchron (Driscoll & Evans, 2016). The single polarity precludes conducting a reversal test. The tilt of the strata are similar between the sections which precludes a meaningful fold test. A baked contact test was conducted by Weil et al. (2003) for an Unkar intrusion (the Lizard Dike) where it intrudes the Dox Formation near Basalt Canyon. The results show a partially positive baked contact test where the Dox Formation near the dike carries stable paleomagnetic remanence that have directions similar to that of the dike. However, the Dox Formation samples collected far away from the dike do not carry stable remanence. This partially positive result supports the interpretation that the magnetization of the Lizard Dike was acquired during cooling of the intrusion. However, it is unclear whether the Lizard Dike is cogenetic with the ca. 1,098 Ma mafic intrusions such as those sills sampled as UI4 and UI5 in this study, or a feeder for the ca. 1,082 Ma Cardenas Basalt. Thermochronological data suggest that rocks of the Grand Canyon have experienced only mild heating since the emplacement of the Cardenas Basalt. ^{40}Ar-^{39}Ar K-feldspar thermochronology data from the crystalline basement of the Grand Canyon show that there could not have been a

21699356, 2024, 10, Downloaded from https://agupubs.onlinelibrary.wiley.com/doi/10.1029/2024JB029036 by Yiming Zhang - University Of Minnesota Lib , Wiley Online Library on [19/10/2024]. See the Terms and Conditions (https://onlinelibrary.wiley.com/terms-and-conditions) on Wiley Online Library for rules of use; OA articles are governed by the applicable Creative Commons License

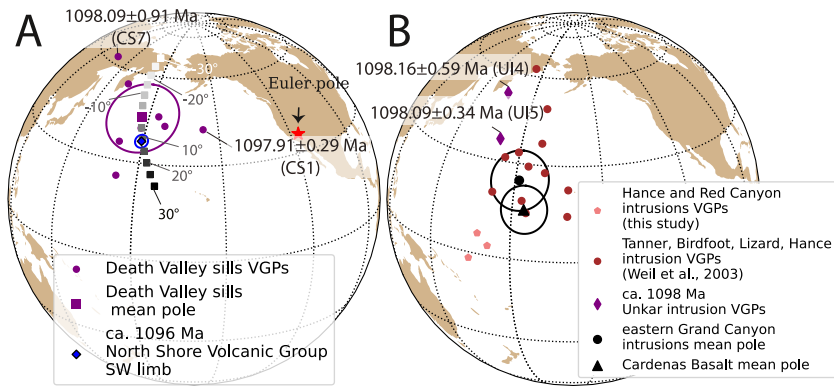

Figure 8. (a) Virtual geomagnetic poles (VGPs) from the Death Valley mafic sills and the associated mean paleomagnetic pole plotted in context of the paleomagnetic pole position of the ca. 1,096 Ma North Shore Volcanic Group southwest sequence pole from Swanson-Hysell et al. (2019). Variable vertical axis rotations of the mean Death Valley sills pole about an Euler pole located at 35.8°N, −116.4°E are shown. Positive (negative) values represent counterclockwise (clockwise) rotations about the Euler pole. (b) VGPs from mafic intrusions in this study and those developed by Weil et al. (2003). VGPs from the dated sills in the western Grand Canyon are shown as purple diamonds and labeled with their ages. A mean paleomagnetic pole from the eastern Grand Canyon intrusions (red circle VGPs of Weil et al. (2003) and pink pentagon VGPs from this study) is plotted with the Cardenas Basalt pole (based on the mean of VGPs shown in Figure 9).

regional heating event in the canyon that reached a temperature above ∼300°C since ca. 1,250 Ma (Thurston et al., 2024; Timmons et al., 2005). Given that the Grand Canyon mafic sills and the Cardenas Basalt typically show origin-trending characteristic remanence components that unblock above 500°C after the removal of a present day field component (Figure 6), these data add to the confidence that the mafic sills and lavas record primary remanence acquired at the time of emplacement.

In addition, when comparing the mean pole positions from the ca. 1,098 Ma Death Valley sills and the ca. 1,082 Ma Cardenas Basalt with the compiled apparent polar wander path for North America (Evans et al., 2021), neither poles overlaps with known poles of younger ages (Figure S7 in Supporting Information S1). This result adds to our confidence that the characteristic remanence recorded by the mafic intrusions and the lava flows was acquired during cooling after their emplacement.

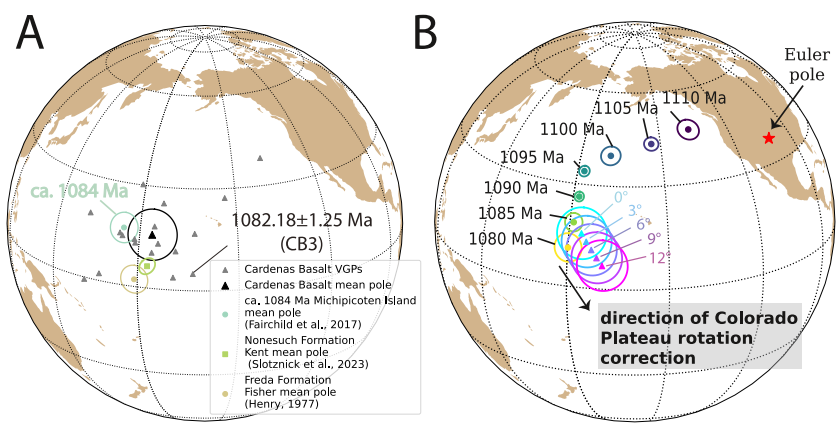

Figure 9. (a) The Virtual geomagnetic poles (VGPs) and mean paleomagnetic pole of the ca. 1,082 Ma Cardenas Basalt are plotted with the ca. 1,084 Ma Michipicoten Island Formation paleomagnetic pole (Fairchild et al., 2017) as well as the ca. 1,075 Ma Nonesuch Formation pole (Slotznick et al., 2023) and lower Freda Formation pole (Henry et al., 1977). The VGP from the dated Cardenas lava flow CB3 is labeled. (b) The Cardenas Basalt mean pole position is corrected for the hypothesized Colorado Plateau rotation with progressively larger rotations about an Euler pole position of −103°E, 37°N (Bryan & Gordon, 1990). The resultant pole positions are plotted in context of the synthesized Keweenawan Track (2 stage pole rotations and true polar wander scenario; Swanson-Hysell et al., 2019). Larger rotations result in less agreement between the Cardenas pole and the pole path based on Midcontinent Rift data.

21699356, 2024, 10, Downloaded from https://agupubs.onlinelibrary.wiley.com/doi/10.1029/2024JB029036 by Yiming Zhang - University Of Minnesota Lib , Wiley Online Library on [19/10/2024]. See the Terms and Conditions (https://onlinelibrary.wiley.com/terms-and-conditions) on Wiley Online Library for rules of use; OA articles are governed by the applicable Creative Commons License

5.2. Insights Into Structural Complexities in Southwestern Laurentia

5.2.1. Neogene Extension and Associated Vertical Axis Rotations in Death Valley Region

The Death Valley region experienced complex deformation associated with extension and shearing during Neogene extensional tectonism (e.g., Wernicke et al., 1988). It has been suggested that tilting associated with generally west-dipping normal faults, as well as vertical axis rotations of crustal blocks associated with conjugate strike-slip fault systems principally accommodated the deformation (e.g., Serpa & Pavlis, 1996). Geologic mapping and associated structural analyses suggest that strike-slip faults are coeval with normal faulting and have a left-lateral sense when they strike eastward or northeastward (e.g., Garlock fault; Figure 2a) and a right-lateral sense when they strike northwestward (e.g., south Death Valley fault; Figure 2a; Pavlis et al., 2014; Serpa & Pavlis, 1996; Wright, 1976). However, the extent to which extension is partitioned between the normal faulting and strike-slip faulting has long been debated (e.g., Burchfiel, 1965; Guth, 1981; Holm et al., 1993; Petronis et al., 2002; Renik & Christie-Blick, 2013; Snow & Wernicke, 1989).

Although tilt-correcting the Death Valley sill directions results in better-grouped site-level directions and supports a primary origin for the magnetization (Figure S6 in Supporting Information S1), it is more challenging to correct for vertical axis rotations in the Death Valley region. In the literature, the amount of rotations experienced by individual range blocks are poorly constrained. Sills CS1, CS2, and CS6 are from Warm Spring Canyon of the Panamint Mountains, which is an east-tilting block now bounded by the right-lateral Panamint Valley fault to the west and the left-lateral Garlock fault to the south (Figure 2; Snow, 2000; Snow & Wernicke, 1989). Stewart (1983) interpreted that the Panamint Range was detached from above the crystalline core of the Black Mountains and translated some 80 km northwest along west dipping low-angle detachment faults. Petronis et al. (2002) developed paleomagnetic data from Miocene intrusive rocks in the central Panamint Range and Miocene volcanic rocks in the eastern part of the range. Their data from the central range show a pole position that overlaps with that expected for no rotation, which they interpreted to indicate minimal amount of vertical axis rotation. They did find a discordance between paleomagnetic declinations developed from Miocene volcanic rocks in the eastern Panamint Range which appear to show substantial clockwise vertical axis rotations since the Miocene (27.6°± 15.2°, calculated based on nine paleomagnetic sites). However, Petronis et al. (2002) cautioned against interpreting there to have been a large vertical axis rotation in the eastern range as their data may undersample paleosecular variation. In the northwest Black Mountains, paleomagnetic data developed from Miocene intrusive rocks and Proterozoic basement rocks have been interpreted to indicate large vertical axis rotations as a result of oroclinal bending associated with right-lateral shear along the Death Valley fault zone (up to ~80°; Holm et al., 1993). However, paleomagnetic data developed from late Miocene igneous rocks in the eastern Panamint Mountains indicate minimal rotations in the region (Petronis et al., 2002). These data led Petronis et al. (2002) to hypothesize that the significant vertical axis rotation interpreted by Holm et al. (1993) could be restricted to the western range where the basement block is sheared along the Death Valley fault zone (Figure 2). In this case, the more southeastern parts of the Black Mountains fault block, where sills CS7, CS8, and CS9 were collected, and distal from the fault zone, may have experienced relatively insignificant vertical axis rotation (Figure 2). In the Nopah Range, where site CS13 was sampled within the crystalline basement (Figure 2), no quantitative constraints exist on the amount of vertical axis rotation. Models that involve no rotation to those with up to 30° of clockwise rotation since the Neogene have all been proposed and interpreted to broadly fit the structural evidence in the region (e.g., Pavlis et al., 2014; Serpa & Pavlis, 1996). Rotation in the Alexander Hills (site CS12) is similarly poorly constrained.

The limited number of paleomagnetic sites from mafic sills in the different range blocks precludes the assessment of vertical axis rotation at each sampling locality (Figure 2a). This limitation is due to the secular variation of the geomagnetic field, which makes it such that single VGPs or low numbers of VGPs do not give accurate or precise estimates of the mean paleomagnetic pole position to be compared to a reference pole path. Until more detailed and quantitative spatial and temporal constraints are developed for the different range blocks of the Death Valley region, it remains inconclusive as to the amount of Neogene vertical axis rotation correction to apply to these Mesoproterozoic sill directions. Given these vertical axis rotation uncertainties, we believe it is the best approach to not include the Death Valley mafic sills paleomagnetic pole into curated paleogeography databases.

However, the tilt-corrected VGPs from the eight mafic sills with well-resolved magnetizations can provide insights into the structural history of the study region when viewed in context of Laurentia's apparent polar wander path in the late Mesoproterozoic. The mean pole position plots at northern high latitudes and overlaps with the

21699356, 2024, 10, Downloaded from https://agupubs.onlinelibrary.wiley.com/doi/10.1029/2024JB029036 by Yiming Zhang - University Of Minnesota Lib , Wiley Online Library on [19/10/2024]. See the Terms and Conditions (https://onlinelibrary.wiley.com/terms-and-conditions) on Wiley Online Library for rules of use; OA articles are governed by the applicable Creative Commons License

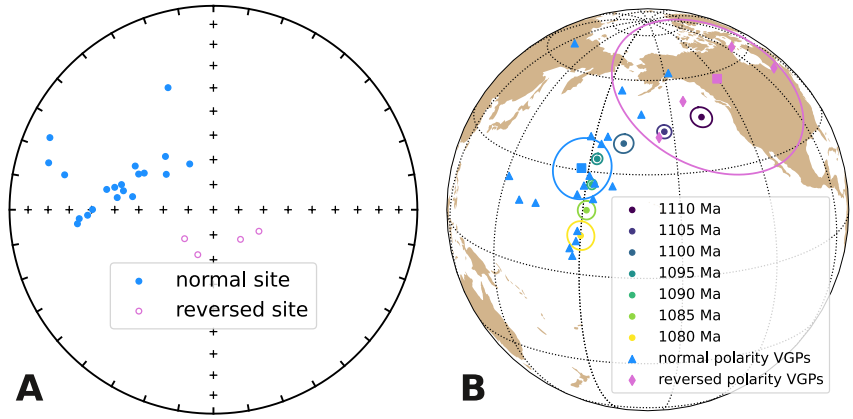

Figure 10. (a) Compiled paleomagnetic directional data developed by Harlan (1993) and Donadini et al. (2011) from mafic sills in central Arizona. The original data are selected with some recalculated such that each site included in this compilation is an individual cooling unit. Some sills record a reversed polarity with steep inclinations (orchid), while the other sills record a normal polarity with shallower inclinations (blue). The compiled data are in Table S3 in Supporting Information S1. (b) Virtual geomagnetic poles of individual cooling units and mean paleomagnetic poles of the central Arizona mafic sills are plotted in context of the synthesized Keweenawan Track of Swanson-Hysell et al. (2019) (two stage pole with true polar wander scenario). The mean pole position of sills with reversed polarity is close to the older end of the Keweenawan Track while the mean normal-polarity pole plots close to the expected pole position ca. 1,095 Ma.

paleomagnetic pole of the ca. 1,096 Ma North Shore Volcanic Group southwest sequence (Figure 8a; Swanson-Hysell et al., 2019). The overlapping pole positions between the ca. 1,098 Ma Death Valley sills mean pole and poles from rocks of similar age in the Midcontinent Rift of the continental interior indicate that any vertical axis rotations were not large enough to have displaced the pole from the path (<30°; Figure 8a). The pole position is also similar to that developed from normal polarity mafic sills in central Arizona (Figure 10).

5.2.2. The Hypothesized Colorado Plateau Rotation

The Grand Canyon is located at the southwestern edge of the Colorado Plateau, which was uplifted, folded, and tilted as a result of compression associated with the subduction of the Farallon plate underneath the North American plate during the late Cretaceous to Paleogene Laramide orogeny (Karlstrom et al., 2022; Karlstrom & Timmons, 2012; Timmons et al., 2012; Yonkee & Weil, 2015). Structural analyses have suggested that the plateau rotated clockwise as a rigid block with respect to cratonic North America due to shear during the orogeny (e.g., Hamilton, 1981; Hamilton, 1988). Efforts to quantitatively constrain the amount of rotation using paleomagnetic data have given different results albeit with agreement that the sense of rotation is clockwise. Kent and Witte (1993) and Steiner (2003) took the approach of developing Mesozoic paleomagnetic poles from the Colorado Plateau and comparing them with reference poles developed from cratonic North America to estimate the amount of rotation. Those studies gave relatively large estimates of interpreted rotations of 13.5 ± 3.5° and 9.0 ± 3.3°, respectively. Challenges exist with the approach of estimating the amount of rotation based on single paleomagnetic pole positions such as issues with age uncertainty between poles and reference pole positions. Garza et al. (1998) and Bryan and Gordon (1990) used approaches based on comparing multiple paleomagnetic poles through the Paleozoic to Mesozoic from on and off the plateau simultaneously and interpreted that the amount of rotation is ∼5°. These smaller estimated rotations are consistent with the structural evidence of a small magnitude of strike-slip translation along the boundary of the Colorado Plateau (e.g., Woodward et al., 1997).

The Cardenas Basalt paleomagnetic pole presents an opportunity of using Mesoproterozoic data to gain insights into Colorado Plateau rotation. Figure 9b shows the mean pole position of the Cardenas Basalt in the context of the synthesized Keweenawan Track apparent polar wander path (two Euler scenario; Swanson-Hysell et al., 2019) which is developed from the Midcontinent Rift region to the northeast of the Colorado Plateau (Figure 2). At 0° of rotation, the Cardenas pole corresponds to the position predicted by the Keweenawan Track. As a progressively larger correction for Colorado Plateau rotation (using an Euler pole at −107°E, 37°N; Bryan and Gordon, 1990) is applied, the Cardenas Basalt pole moves farther away from the Keweenawan Track and no longer overlaps with the expected pole positions at ca. 1,080 Ma after a 6°correction (Figure 9b). This result is consistent with the

21699356, 2024, 10, Downloaded from https://agupubs.onlinelibrary.wiley.com/doi/10.1029/2024JB029036 by Yiming Zhang - University Of Minnesota Lib , Wiley Online Library on [19/10/2024]. See the Terms and Conditions (https://onlinelibrary.wiley.com/terms-and-conditions) on Wiley Online Library for rules of use; OA articles are governed by the applicable Creative Commons License

interpretation that the Colorado Plateau experienced a relatively small amount of rotation (<6°). However, it is not feasible to use the single Cardenas Basalt pole to constrain the amount of Colorado Plateau rotation more precisely than previous estimates, as the Fisher 95% angular uncertainty associated with the pole position itself is 11.8°. Future efforts to constrain Colorado Plateau rotation can incorporate both Mesoproterozoic and Mesozoic poles.

5.3. Chronology of Grand Canyon Region Intrusions and Cardenas Basalt

Weil et al. (2003) developed paleomagnetic data from 13 mafic intrusions (in the eastern Grand Canyon between RM68 and RM78; Figure 2b) as well as three Cardenas Basalt flows at Basalt Canyon. Using the interpretation that the intrusions were time-equivalent with one another and with the lavas, Weil et al. (2003) grouped all paleomagnetic directions from the intrusive and extrusive rocks to calculate a mean paleomagnetic pole position. The pole was assigned an age of 1,090.6 ± 4.5 Ma based on an ^{40}Ar-^{39}Ar age developed from biotite collected within Unkar sedimentary rocks baked by a sill in the western Grand Canyon at RM131 (outside their paleomagnetic study region; Weil et al., 2003). This mean pole position has been included in pole compilations (e.g., Evans et al., 2021) and used to constrain Laurentia's apparent polar wander path in the late Mesoproterozoic.

The recent high-precision zircon U-Pb ages from two sills in western Grand Canyon and the thick Cardenas Basalt flow at Nankoweap Canyon indicate that some of the sills in the Unkar Group are not feeders to the Cardenas Basalt given that their ca. 1,098 Ma ages are ∼16 Myr older than the lavas which erupted ca. 1,082 Ma (Figure 1b; Mohr et al., 2024).

The new paleomagnetic data from the Grand Canyon are consistent with the updated geochronology. Although there are not enough dated ca. 1,098 Ma mafic sills from the Grand Canyon that paleosecular variation can be averaged out and a mean paleomagnetic pole position can be calculated, the VGPs from the two dated mafic sills both plot at high latitudes (Figure 8b). On the other hand, the VGPs of the 18 Cardenas Basalt lava flows are consistent with being Fisher distributed (Figure S8 in Supporting Information S1), with a mean pole position at a lower latitude (Figures 8b and 9). This pole position overlaps with Laurentia's pole path at ca. 1,085 Ma and ca. 1,080 Ma (Figure 9b).

Despite a lack of direct field evidence for feeder dikes, and that the two dated sills in western Grand Canyon cannot be feeders to the lava flows given their older age (Figure 2b), there would have been feeder dikes to the Cardenas Basalt that crosscut older Unkar sedimentary rocks. While high-precision geochronology on individual intrusions would be needed to unambiguously distinguish potential Cardenas feeders from older intrusions, paleomagnetic data have the potential to provide insight given the rapid apparent polar wander of Laurentia at the time. The VGPs of the Red Canyon sill (UI1), Hance dike (UI2), and Hance sill (UI3) are well-grouped at equatorial latitudes (Figure 8b). These poles are close to the younger end of the Keweenawan Track (Figure 9a). Geographically, these intrusions are close to the Cardenas Basalt near Basalt Canyon and far from the dated ca. 1,098 Ma sills (Figure 2b). These data indicate that the Hance intrusions (UI1, UI2, and UI3) could be feeders to the Cardenas Basalt. The Birdfoot dikes, Lizard dikes, and Tanner dikes studied by Weil et al. (2003) are also close to Basalt Canyon (Figure 2b). A mean paleomagnetic pole based on VGPs from these intrusions (i.e., dike data from Weil et al., 2003) and from the Hance intrusions of this study is calculated and shown in Figure 8b. This pole position is similar to that from the Cardenas Basalt. The VGPs from these eastern Grand Canyon intrusions pass a common mean test with the Cardenas Basalts VGPs (Figure 8). This result suggests that some of the eastern Grand Canyon intrusions could be ca. 1,082 Ma feeders to the Cardenas Basalt.

However, some of the individual VGPs of the mafic dikes developed by Weil et al. (2003) plot at relatively high latitudes (Figure 8b). This could indicate that some of them might have been emplaced during the ca. 1,098 Ma pulse of magmatism. New major and trace element geochemical data developed in this study together with trace element data developed from the interior of the Hance sill by Larson et al. (1994) show that the mafic intrusions in the Unkar Group are overall more mafic such that they are basalt while the lavas are dominantly basaltic andesite (Figure S1 in Supporting Information S1). Additionally, the intrusives are more depleted in Rb, Th, and more enriched in Sr relative to the Cardenas Basalt (Figure S2 in Supporting Information S1). Based on these geochemical data, one could interpret that none of the intrusions sampled in this study near Hance Rapids (UI1, UI2, and UI3) fed the Cardenas lava flows and that they could be of different ages. High-precision geochronology data for individual units can help resolve the ambiguity in the relationship between the intrusions and Cardenas Basalt.

21699356, 2024, 10, Downloaded from https://agupubs.onlinelibrary.wiley.com/doi/10.1029/2024JB029036 by Yiming Zhang - University Of Minnesota Lib , Wiley Online Library on [19/10/2024]. See the Terms and Conditions (https://onlinelibrary.wiley.com/terms-and-conditions) on Wiley Online Library for rules of use; OA articles are governed by the applicable Creative Commons License

5.4. Comparison to Mesoproterozoic Paleomagnetic Data From Central Arizona

Paleomagnetic data have been developed from mafic sills in central Arizona that intrude the Apache Group sedimentary rocks (Donadini et al., 2011; Harlan, 1993; Helsley & Spall, 1972). Both Harlan (1993) and Donadini et al. (2011) identified sills in the same region that record normal directions and reversed directions with the reversed directions having steeper inclinations. We compiled paleomagnetic data from these two studies with the goal of having each site be a distinct cooling unit (i.e., an individual sill). Better site-level statistics from intrusions that were sampled by both studies were preferentially used. The resultant compilation is provided in Table S3 in Supporting Information S1. The individual site-level directions, corresponding VGP positions, and overall mean directions and poles are recalculated by polarity and plotted in Figure 10.

The compiled mean pole position of the normal-polarity mafic sills in central Arizona plots near the expected pole position of Laurentia ca. 1,095 Ma based on data from the Midcontinent Rift rocks (Figure 10; Swanson-Hysell et al., 2019). However, the distribution of the normal-polarity VGP positions is distinct from a Fisher distribution (R. Fisher, 1953). Given that these VGPs show an elongate distribution along the Keweenawan Track (Figure 10), we hypothesize that not all sills were emplaced during the same magmatic episode. However, the sills record a normal polarity and one sill yielded a U-Pb baddeleyite age of 1,088 ± 11 Ma (Bright et al., 2014), which has an uncertainty that overlaps with an CA-ID-TIMS zircon U-Pb age of 1,097.97 ± 0.12 Ma from a subhorizonal diabase sill in Salt River Canyon (Mohr et al., 2024). This indicates that some of the sills could be coeval with the ca. 1,098 Ma mafic sills in Death Valley and Grand Canyon. More precise radiometric dates paired with paleomagnetic data are needed from these sills.

Despite the small number of known occurrences, the central Arizona sills with steep negative inclinations have a mean pole position distinct from that of the normal-polarity sills (Figure 10). The mean pole plots near the older end of the Keweenawan Track, indicating a high paleolatitude for Laurentia at the time of their emplacement (Figure 10). This configuration corresponds with the stable high-latitude position of Laurentia between ca. 1,140 and 1,105 Ma (Ernst & Buchan, 1993; Piispa et al., 2018; Swanson-Hysell, 2021). A reversed polarity is also consistent with the Alona Bay reversed polarity zone which has been identified during the onset of magmatism in the Midcontinent Rift (Swanson-Hysell et al., 2019). In addition to there being a linkage between a SWLLIP plume that spread to the Midcontinent Rift ca. 1,098 to 1,096 Ma, as hypothesized in Mohr et al. (2024), it is possible that a plume upwelling under Laurentia at the onset of Midcontinent Rift development led to magmatism in both regions. To assess such temporal and dynamic connections, more precise ages of these reversed-polarity sills are needed.

5.5. New Poles From Southwestern Laurentia Support Rapid Plate Motion

Statistically indistinguishable high-precision U-Pb zircon ages from three sills in Death Valley, two sills in the Grand Canyon, and a sill in central Arizona were interpreted in Mohr et al. (2024) to be consistent with decompression melting of an upwelling mantle plume ca. 1,098 Ma. This interpretation based on geochronology is consistent with previously developed geochemical data that suggest similar magmatic sources for these intrusions (Hammond, 1986; Howard, 1991). The hypothesis of these sills being sourced from a mantle plume predicts that other thick sills in the region associated with the SWLLIP were also emplaced ca. 1,098 Ma. Paleomagnetic directional data can provide another avenue to gain chronological insight on mafic units for which geochronology data have not been or cannot be developed. Rapid changes in Laurentia's pole position between ca. 1,110 and 1,070 Ma (Swanson-Hysell et al., 2019) enable such data to provide more informative temporal constraints than at many other time intervals.

The new paleomagnetic data from the dated sills in the Death Valley region and in the Grand Canyon are consistent with their high-precision U-Pb zircon ages. The 1,097.91 ± 0.29 Ma CS1 sill and the 1,098.09 ± 0.91 Ma CS7 sill in Death Valley and the 1,098.16 ± 0.59 Ma UI4 sill and 1,098.09 ± 0.34 Ma UI5 sill in Grand Canyon have similar VGP positions at high latitudes in present-day coordinates (Figures 8a and 8b). The new paleomagnetic data further show that six additional undated sills in the Death Valley region have directions that are similar to those from the ca. 1,098 Ma dated sills (Figures 7 and 8). Figure 8a shows the mean pole position calculated for all the Death Valley region sills. The mean pole overlaps within uncertainty with the pole position of the ca. 1,096 Ma North Shore Volcanic Group upper southwest sequence of the Midcontinent Rift (Figure 8a; Swanson-Hysell et al., 2019), which leads to the reconstructed position of Laurentia shown in Figure 11. Although the paleomagnetic data of the Death Valley sills have directional uncertainties associated with potential

21699356, 2024, 10, Downloaded from https://agupubs.onlinelibrary.wiley.com/doi/10.1029/2024JB029036 by Yiming Zhang - University Of Minnesota Lib , Wiley Online Library on [19/10/2024]. See the Terms and Conditions (https://onlinelibrary.wiley.com/terms-and-conditions) on Wiley Online Library for rules of use; OA articles are governed by the applicable Creative Commons License

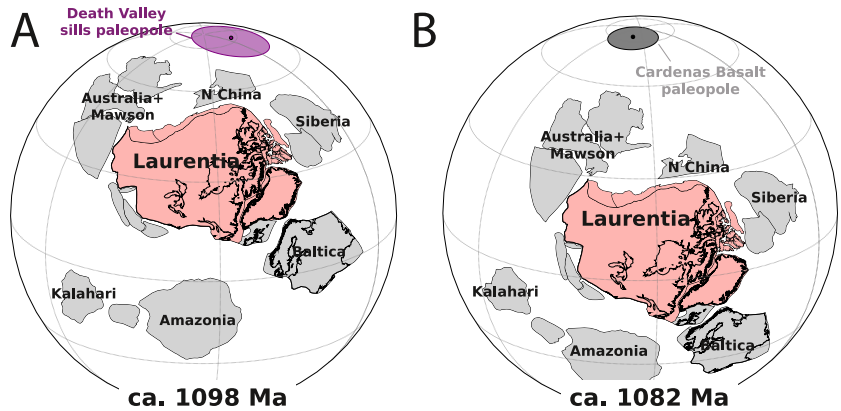

Figure 11. (a) Global paleogeography reconstruction for ca. 1,098 Ma. The Rodinia configuration follows the reconstruction in Swanson-Hysell et al. (2023) with the position of Laurentia constrained by poles from the Midcontinent Rift. The mean pole position of the Death Valley mafic sills is plotted in purple showing the uncertainty overlapping with the spin axis. (b) Global paleogeography reconstruction for ca. 1,082 Ma. The mean pole position of the Cardenas Basalt is plotted in gray and rotated along with Laurentia at this time. The A_{95} uncertainty cone associated with the rotated pole position overlaps with the spin axis.

vertical axis block rotations, these structural complexities do not take away the interpretation that the steep downward inclinations (Figures 6 and 7) are compatible with a ca. 1,098 Ma age.

The paleomagnetic pole position of the ca. 1,082 Ma Cardenas Basalt plots at a lower latitude distinct from that of the ca. 1,098 Ma mafic sills in Death Valley and the western Grand Canyon (Figures 8b and 9a). Instead, the Cardenas Basalt pole is close to the paleomagnetic pole of the Michipicoten Island Formation of the Midcontinent Rift whose age is tightly bracketed to be between 1,084.35 ± 0.20 Ma and 1,083.52 ± 0.23 Ma (Fairchild et al., 2017; Figure 9a). In addition, the Cardenas Basalt pole is close to the ca. 1,075 Ma paleomagnetic poles of the Nonesuch and Freda Formations (Henry et al., 1977; Slotznick et al., 2023) of the Midcontinent Rift Oronto Group (Figure 9a). That these localities ∼2,500 km apart yield overlapping pole positions when their poles are calculated under the assumption of a time-averaged dipolar field supports interpretations that the field was a stable dipole ca. 1,080 Ma. Although there is uncertainty in the Cardenas pole position associated with hypothesized rotation of the Colorado Plateau in the Mesozoic/Cenozoic (Figure 9b; e.g. Bryan and Gordon, 1990), the implied low paleolatitude of Laurentia is unaffected by such uncertainty (Figure 11).

Overall, the large arc distance between the ca. 1,098 Ma and the ca. 1,082 Ma poles from southwestern Laurentia supports the interpretation based on Midcontinent Rift data that Laurentia experienced rapid plate motion from high latitudes toward the equator in the late Mesoproterozoic (Davis & Green, 1997; Swanson-Hysell et al., 2009; Figure 11). This rapid motion is associated with the closure of the Unimos Ocean which culminated in the onset of Grenvillian collisional orogenesis (Swanson-Hysell et al., 2023).

5.6. Outlook for Future Work in the Southwestern Laurentia

The high-precision geochronology data developed by Mohr et al. (2024) revise the southwestern Laurentia large igneous province to feature the emplacement of ca. 1,098 Ma thick mafic intrusions (often >100 m in thickness; Wright and Troxel, 1967) from eastern California to central Arizona. The indistinguishable ages from these thick mafic intrusions across a large areal extent reveal the voluminous and rapid nature of emplacement of the magmatic pulse of the SWLLIP. This large igneous province could include more undated mafic intrusions that could be constrained with paleomagnetic data. Bright et al. (2014) suggested that some mafic sills in New Mexico could also be a part of the SWLLIP, but the available geochronology data does not have the resolution to conclusively test this hypothesis. In Figure 1a, we present an updated version of the areal extent of the SWLLIP as being defined by the ca. 1,098 Ma geochronologically constrained mafic magmatism.

Both geochronology and paleomagnetic data indicate that the Cardenas Basalt in the Grand Canyon was emplaced during a distinct episode of magmatism younger than the SWLLIP mafic sills. However, whether the emplacement of the lava flows is associated with a localized event or another period of large igneous province

21699356, 2024, 10, Downloaded from https://agupubs.onlinelibrary.wiley.com/doi/10.1029/2024JB029036 by Yiming Zhang - University Of Minnesota Lib , Wiley Online Library on [19/10/2024]. See the Terms and Conditions (https://onlinelibrary.wiley.com/terms-and-conditions) on Wiley Online Library for rules of use; OA articles are governed by the applicable Creative Commons License

style magmatism remains to be tested. One mafic sill in the Dead Mountains of eastern California yielded a weighted mean zircon U-Pb age of 1,082.60 ± 0.30 Mohr et al. (2024), which is indistinguishable with the 1,082.18 ± 1.25 Ma age of the Cardenas Basalt (Figure 1b). These ages indicate that the ca. 1,082 Ma mafic magmatism could have stretched over at least 300 km. Over how large of a region did this ca. 1,082 Ma magmatism occur?

The paleomagnetic pole of the Cardenas Basalt can help further constrain the Keweenawan Track given that it is younger than any pole developed from Midcontinent Rift volcanics. Currently, the younger end of the Keweenawan Track is constrained by the ca. 1,084 Ma lava flows of the Michipicoten Island Formation and the ca. 1,080–1,050 Ma Nonesuch Formation and Freda Formation of the Oronto Group (Swanson-Hysell et al., 2019). Uncertainties associated with correcting for inclination shallowing in sedimentary records and constraining the age of detrital remanence magnetization have led to the post-1085 Ma portion of the path to be less constrained than that from ca. 1,110 to 1,085 Ma. The new temporally constrained Cardenas Basalt pole adds a valuable new constraint to Laurentia's database of paleomagnetic poles as it is younger than the Michipicoten Island Formation and in a similar position. Additionally, as a pole developed from well-behaved volcanic rocks, no correction for inclination shallowing is necessary for the Cardenas Basalt. Once the amount of Colorado Plateau rotation and the associated uncertainty is better constrained, an updated Keweenawan Track can be developed using the new site-based resampling approach of Gallo et al. (2023). This method has the machinery to incorporate uncertainties in pole position, geochronology, as well as the magnitude of Colorado Plateau rotation correction into a synthesized path.

Data Availability Statement

The paleomagnetic data developed in this study are archived in the MagIC database (Zhang et al., 2024b). The code implementing the analysis and developing the visualizations of this study are documented within Jupyter notebooks (Kluyver et al., 2016) that are archived on Zenodo (Zhang et al., 2024a). The computational environment used for running these notebooks and conducting the analysis can be reproduced using the environment.yml file within the repository. Instructions associated with recreating this computational environment can be found in the README.md file within the repository. Analyses were performed using the Python packages NumPy (Harris et al., 2020), PmagPy (Tauxe et al., 2016), and Pyrolite (Williams et al., 2020). Figures were created using Matplotlib (Hunter, 2007) and Cartopy (Met Office, 2010).

Acknowledgments
Project research was funded by NSF CAREER Grant EAR-1847277 to N.L.S.-H. Additional research support came from an H2H8 research Grant to Y.Z. as well as a UC Berkeley summer undergraduate research fellowship and a UC Berkeley Department of Earth Science Ramsden grant to N.S.A. We thank participants in the 2021 Grand Canyon Supergroup field forum for stimulating interactions in the canyon. National Park Service Permits for sampling within Grand Canyon National Park and Death Valley National Park are gratefully acknowledged.

References

Barth, A. P., Wooden, J. L., & Coleman, D. S. (2001). SHRIMP-RG U-Pb zircon geochronology of Mesoproterozoic metamorphism and plutonism in the southwesternmost United States. *The Journal of Geology*, *109*(3), 319–327. https://doi.org/10.1086/319975

Barth, A. P., Wooden, J. L., Coleman, D. S., & Fanning, C. M. (2000). Geochronology of the Proterozoic basement of southwesternmost North America, and the origin and evolution of the Mojave crustal province. *Tectonics*, *19*(4), 616–629. https://doi.org/10.1029/1999tc001145

Barth, A. P., Wooden, J. L., Coleman, D. S., & Vogel, M. B. (2009). Assembling and disassembling California: A zircon and monazite geochronologic framework for Proterozoic crustal evolution in southern California. *The Journal of Geology*, *117*(3), 221–239. https://doi.org/10.1086/597515

Beus, S. S., Rawson, R. R., Dalton, R. O., Stevenson, G. M., Reed, S., Daneker, T. M., et al. (1974). Preliminary report on the unkar group (Precambrian) in Grand Canyon, Arizona. In T. Karlstrom, G. Swann, & R. Eastwood (Eds.), *Geology of Northern Arizona, Part I, Regional Studies: Flagstaff, Arizona* (Vol. 1, pp. 34–53). Geological Society of America, Rocky Mountain Section Meeting.

Billingsley, G. H. (2000). *Geologic map of the Grand Canyon 30'x 60'quadrangle, Coconino and Mohave Counties, northwestern Arizona*. (Tech. Rep.). US Geological Survey.

Billingsley, G. H., & Wellmeyer, J. L. (2003). *Geologic map of the Mount Trumbull 30'X 60' Quadrangle, Mohave and Coconino Counties, Northwestern Arizona*. (Tech. Rep.). US Geological Survey.

Bright, R. M., Amato, J. M., Denyszyn, S. W., & Ernst, R. E. (2014). U-Pb geochronology of 1.1 Ga diabase in the southwestern United States: Testing models for the origin of a post-Grenville large igneous province. *Lithosphere*, *6*(3), 135–156. https://doi.org/10.1130/l335.1

Bryan, P., & Gordon, R. G. (1990). Rotation of the Colorado Plateau: An updated analysis of paleomagnetic poles. *Geophysical Research Letters*, *17*(10), 1501–1504. https://doi.org/10.1029/gl017i010p01501

Burchfiel, B. C. (1965). Structural geology of the Specter Range quadrangle, Nevada, and its regional significance. *Geological Society of America Bulletin*, *76*(2), 175. https://doi.org/10.1130/0016-7606(1965)76[175:sgotsr]2.0.co;2

Burchfiel, B. C., Cowan, D. S., & Davis, G. A. (1992). Tectonic overview of the Cordilleran orogen in the western United States. In *The Cordilleran Orogen* (pp. 407–414). Geological Society of America. https://doi.org/10.1130/dnag-gna-g3.407

Burchfiel, B. C., Pelton, P. J., & Sutter, J. (1970). An early Mesozoic deformation belt in south-central Nevada-southeastern California. *Geological Society of America Bulletin*, *81*(1), 211. https://doi.org/10.1130/0016-7606(1970)81[211:aemdbi]2.0.co;2

Calzia, J., & Rämö, O. (2000). Late Cenozoic crustal extension and magmatism, southern Death Valley region, California. In *GSA field guide 2: Great basin and Sierra Nevada* (pp. 135–164). Geological Society of America. https://doi.org/10.1130/0-8137-0002-7.135

Davis, D. W., & Green, J. C. (1997). Geochronology of the North American Midcontinent Rift in western Lake Superior and implications for its geodynamic evolution. *Canadian Journal of Earth Sciences*, *34*(4), 476–488. https://doi.org/10.1139/e17-039

21699356, 2024, 10, Downloaded from https://agupubs.onlinelibrary.wiley.com/doi/10.1029/2024JB029036 by Yiming Zhang - University Of Minnesota Lib , Wiley Online Library on [19/10/2024]. See the Terms and Conditions (https://onlinelibrary.wiley.com/terms-and-conditions) on Wiley Online Library for rules of use; OA articles are governed by the applicable Creative Commons License

Deenen, M. H. L., Langereis, C. G., van Hinsbergen, D. J. J., & Biggin, A. J. (2011). Geomagnetic secular variation and the statistics of palaeomagnetic directions. *Geophysical Journal International*, *186*(2), 509–520. https://doi.org/10.1111/j.1365-246x.2011.05050.x

Dehler, C., Gehrels, G., Porter, S., Heizler, M., Karlstrom, K., Cox, G., et al. (2017). Synthesis of the 780–740 Ma Chuar, Uinta Mountain, and Pahrump (ChUMP) groups, western USA: Implications for Laurentia-wide cratonic marine basins. *Geological Society of America Bulletin*, *129*(5–6), 607–624. https://doi.org/10.1130/b31532.1

Dehler, C., Schmitz, M., Bullard, A., Porter, S., Timmons, M., Karlstrom, K., & Cothren, H. (2023). Precise U-Pb age models refine Neoproterozoic western Laurentian rift initiation, correlation, and Earth system changes. *Precambrian Research*, *396*, 107156. https://doi.org/10.1016/j.precamres.2023.107156

Donadini, F., Pesonen, L. J., Korhonen, K., Deutsch, A., Harlan, S., Heaman, L., et al. (2012). Symmetric and asymmetric reversals in the 1.1 Ga central Arizona diabases: The debate continues. In *Supercontinent symposium* (pp. 35–36).

Donadini, F., Pesonen, L. J., Korhonen, K., Deutsch, A., & Harlan, S. S. (2011). Paleomagnetism and paleointensity of the 1.1 Ga old diabase sheets from central Arizona. *Geophysica*, *47*(1–2), 3–30.

Driscoll, P. E., & Evans, D. A. (2016). Frequency of Proterozoic geomagnetic superchrons. *Earth and Planetary Science Letters*, *437*, 9–14. https://doi.org/10.1016/j.epsl.2015.12.035

Elston, D. P. (1989). Middle and late Proterozoic Grand Canyon Supergroup, Arizona. In *Geology of Grand Canyon, Northern Arizona (with Colorado River Guides): Lee Ferry to Pierce Ferry, Arizona* (pp. 94–105). American Geophysical Union. https://doi.org/10.1029/ft115p0094

Elston, D. P., & Scott, G. R. (1973). Paleomagnetism of some Precambrian basaltic flows and red beds, Eastern Grand Canyon, Arizona. *Earth and Planetary Science Letters*, *18*(2), 253–265. https://doi.org/10.1016/0012-821x(73)90064-2

Elston, D. P., & Scott, G. R. (1976). Unconformity at the Cardenas-Nankoweap contact (Precambrian), Grand Canyon Supergroup, northern Arizona. *Geological Society of America Bulletin*, *87*(12), 1763. https://doi.org/10.1130/0016-7606(1976)87⟨1763:uatccp⟩2.0.co;2

Ernst, R. E., & Buchan, K. L. (1993). Paleomagnetism of the Abitibi dyke swarm, southern Superior province, and implications for the Logan Loop. *Canadian Journal of Earth Sciences*, *30*(9), 1886–1897. https://doi.org/10.1139/e93-167

Evans, D. A. D. (2021). Meso-neoproterozoic Rodinia supercycle. In *Ancient supercontinents and the paleogeography of earth* (pp. 549–576). Elsevier. https://doi.org/10.1016/b978-0-12-818533-9.00006-0

Evans, D. A. D., Pesonen, L. J., Eglington, B. M., Elming, S.-Å., Gong, Z., Li, Z.-X., et al. (2021). An expanding list of reliable paleomagnetic poles for Precambrian tectonic reconstructions. In *Ancient supercontinents and the paleogeography of earth* (pp. 605–639). Elsevier. https://doi.org/10.1016/b978-0-12-818533-9.00007-2

Fairchild, L. M., Swanson-Hysell, N. L., Ramezani, J., Sprain, C. J., & Bowring, S. A. (2017). The end of Midcontinent Rift magmatism and the paleogeography of Laurentia. *Lithosphere*, *9*(1), 117–133. https://doi.org/10.1130/l580.1

Fisher, R. (1953). Dispersion on a sphere. *Proceedings of the Royal Society A: Mathematical, Physical and Engineering Sciences*, *217*(1130), 295–305. https://doi.org/10.1098/rspa.1953.0064

Gallo, L. C., Domeier, M., Sapienza, F., Swanson-Hysell, N. L., Vaes, B., Zhang, Y., et al. (2023). Embracing uncertainty to resolve polar wander: A case study of Cenozoic North America. *Geophysical Research Letters*, *50*(11), e2023GL103436. https://doi.org/10.1029/2023GL103436

Garza, R. S. M., Acton, G. D., & Geissman, J. W. (1998). Carboniferous through Jurassic paleomagnetic data and their bearing on rotation of the Colorado plateau. *Journal of Geophysical Research*, *103*(B10), 24179–24188. https://doi.org/10.1029/98jb02053

Green, G. N. (1992). *The digital geologic map of Colorado in ARC/INFO format*. (Tech. Rep.). U.S. Geological Survey.

Gundy, C. E. V. (1951). Nankoweap group of the Grand Canyon Algonkian of Arizona. *Geological Society of America Bulletin*, *62*(8), 953. https://doi.org/10.1130/0016-7606(1951)62[953:ngotgc]2.0.co;2

Guth, P. L. (1981). Tertiary extension north of the Las Vegas Valley shear zone, Sheep and Desert Ranges, Clark County, Nevada. *Geological Society of America Bulletin*, *92*(10), 763. https://doi.org/10.1130/0016-7606(1981)92⟨763:tenotl⟩2.0.co;2

Hamilton, W. B. (1981). Plate-tectonic mechanism of Laramide deformation. *Contributions to Geology University of Wyoming*, *19*(2), 87–92.

Hamilton, W. B. (1988). Laramide crustal shortening. In *Interaction of the rocky Mountain foreland and the cordilleran thrust belt* (pp. 27–40). Geological Society of America. https://doi.org/10.1130/mem171-p27

Hammond, J. G. (1983). Late Precambrian diabase intrusions in the southern Death Valley region. California: Their petrology. Geochemistry, and tectonic significance [Ph.D.]. ProQuest Dissertations and Theses (DP28563). (p. 293).

Hammond, J. G. (1986). Geochemistry and petrogenesis of Proterozoic diabase in the southern Death Valley region of California. *Contributions to Mineralogy and Petrology*, *93*(3), 312–321. https://doi.org/10.1007/bf00389390

Hammond, J. G., & Wooden, J. (1990). Isotopic constraints on the petrogenesis of Proterozoic diabase in southwestern USA. *International dyke conference*, *2*, 145–156.

Harlan, S. S. (1993). Paleomagnetism of Middle Proterozoic diabase sheets from central Arizona. *Canadian Journal of Earth Sciences*, *30*(7), 1415–1426. https://doi.org/10.1139/e93-122

Harris, C. R., Millman, K. J., van der Walt, S. J., Gommers, R., Virtanen, P., Cournapeau, D., et al. (2020). Array programming with NumPy. *Nature*, *585*(7825), 357–362. https://doi.org/10.1038/s41586-020-2649-2

Heaman, L. M., & Grotzinger, J. P. (1992). 1.08 Ga diabase sills in the Pahrump Group, California: Implications for development of the Cordilleran miogeocline. *Geology*, *20*(7), 637. https://doi.org/10.1130/0091-7613(1992)020⟨0637:gdsitp⟩2.3.co;2

Helsley, C. E., & Spall, H. (1972). Paleomagnetism of 1140 to 1150 million-year diabase sills from Gila County, Arizona. *Journal of Geophysical Research*, *77*(11), 2115–2128. https://doi.org/10.1029/jb077i011p02115

Hendricks, J. D. (1972). *Younger precambrian basaltic rocks of the Grand Canyon, Arizona (unpublished doctoral dissertation)*. Northern Arizona University.

Hendricks, J. D. (1989). Petrology and chemistry of igneous rocks of Middle Proterozoic Unkar Group, Grand Canyon Supergroup, northern Arizona. In *Geology of Grand Canyon, Northern Arizona (with Colorado River Guides): Lee Ferry to Pierce Ferry, Arizona* (pp. 106–116). American Geophysical Union. https://doi.org/10.1029/ft115p0106

Hendricks, J. D., Lucchitta, I., Karlstrom, T., Swann, G., & Eastwood, R. (1974). Upper Precambrian igneous rocks of the Grand Canyon, Arizona. In *Geology of northern arizona* (pp. 65–86).

Henry, S. G., Mauk, F. J., & der Voo, R. V. (1977). Paleomagnetism of the upper Keweenawan sediments: The Nonesuch Shale and Freda Sandstone. *Canadian Journal of Earth Sciences*, *14*(5), 1128–1138. https://doi.org/10.1139/e77-103

Holm, D. K., Geissman, J. W., & Wernicke, B. (1993). Tilt and rotation of the footwall of a major normal fault system: Paleomagnetism of the Black Mountains, Death Valley extended terrane, California. *Geological Society of America Bulletin*, *105*(10), 1373–1387. https://doi.org/10.1130/0016-7606(1993)105⟨1373:tarotf⟩2.3.co;2

Howard, K. A. (1991). Intrusion of horizontal dikes: Tectonic significance of Middle Proterozoic diabase sheets widespread in the upper crust of the southwestern United States. *Journal of Geophysical Research*, *96*(B7), 12461–12478. https://doi.org/10.1029/91jb00112

21699356, 2024, 10, Downloaded from https://agupubs.onlinelibrary.wiley.com/doi/10.1029/2024JB029036 by Yiming Zhang - University Of Minnesota Lib , Wiley Online Library on [19/10/2024]. See the Terms and Conditions (https://onlinelibrary.wiley.com/terms-and-conditions) on Wiley Online Library for rules of use; OA articles are governed by the applicable Creative Commons License

Hunter, J. D. (2007). Matplotlib: A 2D graphics environment. *Computing in Science & Engineering*, *9*(3), 90–95. https://doi.org/10.1109/mcse.2007.55

Huntoon, P., Billingsley, G., Sears, J., Ilg, B., Karlstrom, K., Williams, M., & Hawkins, D. (1996). Geologic map of the eastern Grand Canyon National Park (Tech. Rep.). *Grand Canyon Association and Museum of Northern Arizona*.

Karlstrom, K. E., & Humphreys, E. D. (1998). Persistent influence of Proterozoic accretionary boundaries in the tectonic evolution of southwestern North America: Interaction of cratonic grain and mantle modification events. *Rocky Mountain Geology*, *33*(2), 161–179. https://doi.org/10.2113/33.2.161

Karlstrom, K. E., & Timmons, J. M. (2012). Faulting and uplift in the Grand Canyon region. In *Grand Canyon Geology: Two Billion Years of Earth's history*. Geological Society of America. https://doi.org/10.1130/2012.2489(06

Karlstrom, K. E., Wilgus, J., Thacker, J. O., Schmandt, B., Coblentz, D., & Albonico, M. (2022). Tectonics of the Colorado Plateau and its margins. *Annual Review of Earth and Planetary Sciences*, *50*(1), 295–322. https://doi.org/10.1146/annurev-earth-032320-111432

Kent, D. V., & Witte, W. K. (1993). Slow apparent polar wander for North America in the Late Triassic and large Colorado Plateau rotation. *Tectonics*, *12*(1), 291–300. https://doi.org/10.1029/92tc01966

Kirschvink, J. L. (1980). The least-squares line and plane and the analysis of palaeomagnetic data. *Geophysical Journal International*, *62*(3), 699–718. https://doi.org/10.1111/j.1365-246x.1980.tb02601.x

Kluyver, T., Ragan-Kelley, B., Pérez, F., Granger, B. E., Bussonnier, M., Frederic, J., et al. (2016). *Jupyter Notebooks-a publishing format for reproducible computational workflows* (Vol. 2016, pp. 87–90). Elpub.

Labotka, T. C., Albee, A. L., Lanphere, M. A., & McDowell, S. D. (1980). Stratigraphy, structure, and metamorphism in the central Panamint Mountains (Telescope Peak quadrangle), Death Valley area, California. *GSA Bulletin*, *91*(3_Part_II), 843–933. https://doi.org/10.1130/gsab-p2-91-843

Labotka, T. C., Warasila, R. L., & Spangler, R. R. (1985). Polymetamorphism in the Panamint Mountains, California: A ^{39}Ar-^{40}Ar study. *Journal of Geophysical Research*, *90*(B12), 10359–10371. https://doi.org/10.1029/jb090ib12p10359

Lanphere, M. A. (1964). Geochronologic studies in the eastern Mojave Desert, California. *The Journal of Geology*, *72*(4), 381–399. https://doi.org/10.1086/626997

Larson, E., Patterson, P., & Mutschler, F. (1994). Lithology, chemistry, age, and origin of the Proterozoic Cardenas Basalt, Grand Canyon, Arizona. *Precambrian Research*, *65*(1–4), 255–276. https://doi.org/10.1016/0301-9268(94)90108-2

Lucchitta, I. (1979). Late Cenozoic uplift of the southwestern Colorado Plateau and adjacent lower Colorado River region. *Tectonophysics*, *61*(1–3), 63–95. https://doi.org/10.1016/0040-1951(79)90292-0

Lucchitta, I., & Hendricks, J. D. (1983). Characteristics, depositional environment, and tectonic interpretations of the Proterozoic Cardenas Lavas, eastern Grand Canyon, Arizona. *Geology*, *11*(3), 177. https://doi.org/10.1130/0091-7613(1983)11⟨177:cdeati⟩2.0.co;2

Macdonald, F. A., Prave, A. R., Petterson, R., Smith, E. F., Pruss, S. B., Oates, K., et al. (2013). The Laurentian record of Neoproterozoic glaciation, tectonism, and eukaryotic evolution in Death Valley, California. *Geological Society of America Bulletin*, *125*(7–8), 1203–1223. https://doi.org/10.1130/b30789.1

Mahon, R. C., Dehler, C. M., Link, P. K., Karlstrom, K. E., & Gehrels, G. E. (2014a). Detrital zircon provenance and paleogeography of the Pahrump Group and overlying strata, Death Valley, California. *Precambrian Research*, *251*, 102–117. https://doi.org/10.1016/j.precamres.2014.06.005

Mahon, R. C., Dehler, C. M., Link, P. K., Karlstrom, K. E., & Gehrels, G. E. (2014b). Geochronologic and stratigraphic constraints on the Mesoproterozoic and Neoproterozoic Pahrump group, Death Valley, California: A record of the assembly, stability, and breakup of Rodinia. *Geological Society of America Bulletin*, *126*(5–6), 652–664. https://doi.org/10.1130/b30956.1

Met Office. (2010). Cartopy: A cartographic python library with a matplotlib interface (computer software manual) [Computer software manual]. https://github.com/SciTools/cartopy

Miller, J. D., & Nicholson, S. W. (2013). Geology and mineral deposits of the 1.1 Ga Midcontinent Rift in the Lake Superior region – An overview. In *Field guide to the copper-nickel-platinum group element deposits of the lake superior region*. Precambrian Research Center.

Mohr, M., Schmitz, M., Swanson-Hysell, N., Karlstrom, K., Macdonald, F., Holland, M., et al. (2024). High-precision U-Pb geochronology links magmatism in the southwestern Laurentia large igneous province and Midcontinent Rift. *Geology*, *52*(3), 193–198. https://doi.org/10.1130/g51786.1

Moskowitz, B. M., Jackson, M., & Kissel, C. (1998). Low-temperature magnetic behavior of titanomagnetites. *Earth and Planetary Science Letters*, *157*(3–4), 141–149. https://doi.org/10.1016/s0012-821x(98)00033-8

Mulder, J. A., Karlstrom, K. E., Fletcher, K., Heizler, M. T., Timmons, J. M., Crossey, L. J., et al. (2017). The syn-orogenic sedimentary record of the Grenville Orogeny in southwest Laurentia. *Precambrian Research*, *294*, 33–52. https://doi.org/10.1016/j.precamres.2017.03.006

Muxworthy, A. R., & McClelland, E. (2000). The causes of low-temperature demagnetization of remanence in multidomain magnetite. *Geophysical Journal International*, *140*(1), 115–131. https://doi.org/10.1046/j.1365-246x.2000.00000.x

Oliveira, A., Schmitz, M., Wall, C., & Hollanda, M. (2022). A bulk annealing and dissolution-based zircon concentration method for mafic rocks. *Chemical Geology*, *120817*, 120817. https://doi.org/10.1016/j.chemgeo.2022.120817

Özdemir, Ö., & Dunlop, D. J. (2006). Magnetic memory and coupling between spin-canted and defect magnetism in hematite. *Journal of Geophysical Research*, *111*(B12). https://doi.org/10.1029/2006jb004555

Pavlis, T. L., Rutkofske, J., Guerrero, F., & Serpa, L. F. (2014). Structural overprinting of Mesozoic thrust systems in eastern California and its importance to reconstruction of Neogene extension in the southern Basin and Range. *Geosphere*, *10*(4), 732–756. https://doi.org/10.1130/ges00993.1

Petronis, M. S., Geissman, J. W., Holm, D. K., Wernicke, B., & Schauble, E. (2002). Assessing vertical axis rotations in large-magnitude extensional settings: A transect across the Death Valley extended terrane, California. *Journal of Geophysical Research*, *107*(B1). https://doi.org/10.1029/2001jb000239

Piispa, E. J., Smirnov, A. V., Pesonen, L. J., & Mitchell, R. H. (2018). Paleomagnetism and geochemistry of ∼1144-Ma lamprophyre dikes, northwestern Ontario: Implications for the North American polar wander and plate velocities. *Journal of Geophysical Research: Solid Earth*, *123*(8), 6195–6214. https://doi.org/10.1029/2018jb015992

Renik, B., & Christie-Blick, N. (2013). A new hypothesis for the amount and distribution of dextral displacement along the Fish Lake Valley-northern Death Valley-Furnace Creek fault zone, California-Nevada. *Tectonics*, *32*(2), 123–145. https://doi.org/10.1029/2012tc003170

Rivers, T. (2015). Tectonic setting and evolution of the Grenville orogen: An assessment of progress over the last 40 years. *Geoscience Canada*, *42*(1), 77–124. https://doi.org/10.12789/geocanj.2014.41.057

Sears, J. W. (1973). Structural geology of the Precambrian Grand Canyon series, Arizona. ProQuest Dissertations and Theses, 100.

Sears, J. W. (1990). Geologic structure of the the Grand Canyon Supergroup. In S. Beus & M. Morales (Eds.), *Grand Canyon Geology*. Oxford University Press.

21699356, 2024, 10, Downloaded from https://agupubs.onlinelibrary.wiley.com/doi/10.1029/2024JB029036 by Yiming Zhang - University Of Minnesota Lib, Wiley Online Library on [19/10/2024]. See the Terms and Conditions (https://onlinelibrary.wiley.com/terms-and-conditions) on Wiley Online Library for rules of use; OA articles are governed by the applicable Creative Commons License

Serpa, L., & Pavlis, T. L. (1996). Three-dimensional model of the late Cenozoic history of the Death Valley region, southeastern California. *Tectonics*, *15*(6), 1113–1128. https://doi.org/10.1029/96tc01633

Shride, A. F. (1967). *Younger Precambrian geology in southern Arizona*. US Geological Survey. https://doi.org/10.3133/pp566

Slotznick, S. P., Swanson-Hysell, N. L., Zhang, Y., Clayton, K. E., Wellman, C. H., Tosca, N. J., & Strother, P. K. (2023). Reconstructing the paleoenvironment of an oxygenated Mesoproterozoic shoreline and its record of life. *GSA Bulletin*. https://doi.org/10.1130/B36634.1

Snow, J. K. (2000). Cenozoic tectonism in the central basin and range: Magnitude, rate, and distribution of upper crustal strain. *American Journal of Science*, *300*(9), 659–719. https://doi.org/10.2475/ajs.300.9.659

Snow, J. K., Asmerom, Y., & Lux, D. R. (1991). Permian-Triassic plutonism and tectonics, Death Valley region, California and Nevada. *Geology*, *19*(6), 629. https://doi.org/10.1130/0091-7613(1991)019⟨0629:ptpatd⟩2.3.co;2

Snow, J. K., & Wernicke, B. (1989). Uniqueness of geological correlations: An example from the Death Valley extended terrain. *Geological Society of America Bulletin*, *101*(11), 1351–1362. https://doi.org/10.1130/0016-7606(1989)101⟨1351:uogcae⟩2.3.co;2

Steiner, M. B. (2003). A cratonic Middle Jurassic paleopole: Callovian-Oxfordian stillstand (J-2 cusp), rotation of the Colorado Plateau, and Jurassic North American apparent polar wander. *Tectonics*, *22*(3). https://doi.org/10.1029/2001tc001284

Stevens, C. H., Stone, P., Dunne, G. C., Greene, D. C., Walker, J. D., & Swanson, B. J. (1997). Paleozoic and Mesozoic evolution of east-central California. *International Geology Review*, *39*(9), 788–829. https://doi.org/10.1080/00206819709465303

Stevenson, G. M., & Beus, S. S. (1982). Stratigraphy and depositional setting of the upper Precambrian Dox Formation in Grand Canyon. *Geological Society of America Bulletin*, *93*(2), 163. https://doi.org/10.1130/0016-7606(1982)93⟨163:sadsot⟩2.0.co;2

Stewart, J. H. (1983). Extensional tectonics in the Death Valley area, California: Transport of the Panamint range structural block 80 km northwestward. *Geology*, *11*(3), 153. https://doi.org/10.1130/0091-7613(1983)11⟨153:etitdv⟩2.0.co;2

Strickland, A., Wooden, J. L., Mattinson, C. G., Ushikubo, T., Miller, D. M., & Valley, J. W. (2013). Proterozoic evolution of the Mojave crustal province as preserved in the Ivanpah Mountains, southeastern California. *Precambrian Research*, *224*, 222–241. https://doi.org/10.1016/j.precamres.2012.09.006

Swanson-Hysell, N. L. (2021). The Precambrian paleogeography of Laurentia. In *Ancient supercontinents and the paleogeography of earth* (pp. 109–153). Elsevier. https://doi.org/10.1016/b978-0-12-818533-9.00009-6

Swanson-Hysell, N. L., Feinberg, J. M., Berquó, T. S., & Maloof, A. C. (2011). Self-reversed magnetization held by martite in basalt flows from the 1.1-billion-year-old Keweenawan rift, Canada. *Earth and Planetary Science Letters*, *305*(1–2), 171–184. https://doi.org/10.1016/j.epsl.2011.02.053

Swanson-Hysell, N. L., Hoaglund, S. A., Crowley, J. L., Schmitz, M. D., Zhang, Y., & Miller, J. D. (2021). Rapid emplacement of massive Duluth complex intrusions within the North American Midcontinent Rift. *Geology*, *49*(2), 185–189. https://doi.org/10.1130/g47873.1

Swanson-Hysell, N. L., Maloof, A. C., Weiss, B. P., & Evans, D. A. D. (2009). No asymmetry in geomagnetic reversals recorded by 1.1-billion-year-old Keweenawan basalts. *Nature Geoscience*, *2*(10), 713–717. https://doi.org/10.1038/ngeo622

Swanson-Hysell, N. L., Ramezani, J., Fairchild, L. M., & Rose, I. R. (2019). Failed rifting and fast drifting: Midcontinent Rift development, Laurentia's rapid motion and the driver of Grenvillian orogenesis. *GSA Bulletin*, *131*(5–6), 913–940. https://doi.org/10.1130/b31944.1

Swanson-Hysell, N. L., Rivers, T., & van der Lee, S. (2023). The late Mesoproterozoic to early Neoproterozoic Grenvillian orogeny and the assembly of Rodinia: Turning point in the tectonic evolution of Laurentia. In *Laurentia: Turning points in the evolution of a continent*. Geological Society of America. https://doi.org/10.1130/2022.1220(14)

Tapani Rämö, O., & Calzia, J. P. (1998). Nd isotopic composition of cratonic rocks in the southern Death Valley region: Evidence for a substantial Archean source component in Mojavia. *Geology*, *26*(10), 891. https://doi.org/10.1130/0091-7613(1998)026⟨0891:nicocr⟩2.3.co;2

Tauxe, L., Shaar, R., Jonestrask, L., Swanson-Hysell, N. L., Minnett, R., Koppers, A. A. P., et al. (2016). PmagPy: Software package for paleomagnetic data analysis and a bridge to the magnetics information Consortium (MagIC) database. *Geochemistry, Geophysics, Geosystems*, *17*(6), 2450–2463. https://doi.org/10.1002/2016gc006307

Thurston, O., Guenthner, W., Karlstrom, K., Heizler, M., Ricketts, J., & McDannell, K. (2024). Deep-time thermal history of the Great unconformity in the Grand Canyon, USA: Combined zircon (U-Th)/He and K-feldspar 40Ar/39Ar thermochronometers. *Geological Society of America Bulletin*. https://doi.org/10.1130/b37358.1

Timmons, J. M., Bloch, J., Fletcher, K., Karlstrom, K. E., Heizler, M., & Crossey, L. J. (2012). The Grand Canyon Unkar Group: Mesoproterozoic basin formation in the continental interior during supercontinent assembly. In *Grand canyon geology: Two billion years of earth's history*. Geological Society of America. https://doi.org/10.1130/2012.2489(02

Timmons, J. M., Karlstrom, K. E., Dehler, C. M., Geissman, J. W., & Heizler, M. T. (2001). Proterozoic multistage (ca. 1.1 and 0.8 Ga) extension recorded in the Grand Canyon Supergroup and establishment of northwest- and north-trending tectonic grains in the southwestern United States. *Geological Society of America Bulletin*, *113*(10), 0163. https://doi.org/10.1130/0016-7606(2001)113⟨0163:pmcage⟩2.0.co;2

Timmons, J. M., Karlstrom, K. E., Heizler, M. T., Bowring, S. A., Gehrels, G. E., & Crossey, L. J. (2005). Tectonic inferences from the ca. 1255–1100 Ma Unkar Group and Nankoweap Formation, Grand Canyon: Intracratonic deformation and basin formation during protracted Grenville orogenesis. *Geological Society of America Bulletin*, *117*(11), 1573. https://doi.org/10.1130/b25538.1

Vervoort, J. D., Wirth, K., Kennedy, B., Sandland, T., & Harpp, K. S. (2007). The magmatic evolution of the Midcontinent rift: New geochronologic and geochemical evidence from felsic magmatism. *Precambrian Research*, *157*(1–4), 235–268. https://doi.org/10.1016/j.precamres.2007.02.019

Walcott, C. D. (1883). Pre-carboniferous strata in the Grand Canyon of the Colorado, Arizona. *American Journal of Science*, *s3–26*(156), 437–442. https://doi.org/10.2475/ajs.s3-26.156.437

Wasserburg, G. J., Albee, A. L., & Lanphere, M. A. (1964). Migration of radiogenic strontium during metamorphism. *Journal of Geophysical Research*, *69*(20), 4395–4401. https://doi.org/10.1029/jz069i020p04395

Wasserburg, G. J., Wetherill, G. W., & Wright, L. A. (1959). Ages in the Precambrian terrane of Death Valley, California. *The Journal of Geology*, *67*(6), 702–708. https://doi.org/10.1086/626628

Weil, A. B., Geissman, J. W., Heizler, M., & Van der Voo, R. (2003). Paleomagnetism of Middle Proterozoic mafic intrusions and upper Proterozoic (Nankoweap) red beds from the lower Grand Canyon Supergroup, Arizona. *Tectonophysics*, *375*(1–4), 199–220. https://doi.org/10.1016/s0040-1951(03)00339-1

Wernicke, B., Axen, G. J., & Snow, J. K. (1988). Basin and Range extensional tectonics at the latitude of Las Vegas, Nevada. *Geological Society of America Bulletin*, *100*(11), 1738–1757. https://doi.org/10.1130/0016-7606(1988)100⟨1738:bareta⟩2.3.co;2

Williams, M., Schoneveld, L., Mao, Y., Klump, J., Gosses, J., Dalton, H., et al. (2020). Pyrolite: Python for geochemistry. *Journal of Open Source Software*, *5*(50), 2314. https://doi.org/10.21105/joss.02314

Woodward, L. A., Anderson, O. J., & Lucas, S. G. (1997). Mesozoic stratigraphic constraints on Laramide right slip on the east side of the Colorado Plateau. *Geology*, *25*(9), 843. https://doi.org/10.1130/0091-7613(1997)025⟨0843:mscolr⟩2.3.co;2

21699356, 2024, 10, Downloaded from https://agupubs.onlinelibrary.wiley.com/doi/10.1029/2024JB029036 by Yiming Zhang - University Of Minnesota Lib , Wiley Online Library on [19/10/2024]. See the Terms and Conditions (https://onlinelibrary.wiley.com/terms-and-conditions) on Wiley Online Library for rules of use; OA articles are governed by the applicable Creative Commons License

Workman, J. B., Menges, C. M., Page, W. R., Taylor, E. M., Ekren, E. B., Rowley, P. D., et al. (2003). *Geologic map of the Death Valley groundwater model area, Nevada and California*. (Tech. Rep.). United States Geological Survey-Nevada. https://doi.org/10.2172/809981

Wright, L. (1976). Late Cenozoic fault patterns and stress fields in the Great Basin and westward displacement of the Sierra Nevada block. *Geology*, *4*(8), 489. https://doi.org/10.1130/0091-7613(1976)4⟨489:lcfpas⟩2.0.co;2

Wright, L., & Troxel, B. (1967). Limitations on right-lateral, strike-slip displacement, Death Valley and Furnace Creek fault zones, California. *Geological Society of America Bulletin*, *78*(8), 933. https://doi.org/10.1130/0016-7606(1967)78[933:lorsdd]2.0.co;2

Wright, L., & Troxel, B. (1968). *Talc deposits of the Southern Death Valley-Kingston range region*. Division of Mines and Geology.

Wright, L., Troxel, B., Williams, E., Roberts, M., & Diehl, P. (1974). *Precambrian sedimentary environments of the Death Valley region, eastern California* (Vol. 106, pp. 7–15). Geologic features of Death Valley, California: California Division of Mines and Geology Special Report.

Wrucke, C. (1966). *Precambrian and Permian rocks in the vicinity of Warm spring Canyon, Panamint Range, California. (Unpublished doctoral dissertation)*. Stanford University.

Wrucke, C., & Shride, A. (1972). Correlation of Precambrian diabase in Arizona and southern California. In *Geological society of America abstracts with programs* (Vol. 4, pp. 265–266).

Wrucke, C., Stone, P., & Stevens, C. (2007). *Geologic map of the Warm spring Canyon Area, Death Valley National Park, Inyo County, California, with a discussion of the regional significance of the stratigraphy and structure*. (Tech. Rep.). Geological Survey (US).

Yonkee, W. A., & Weil, A. B. (2015). Tectonic evolution of the Sevier and Laramide belts within the North American Cordillera orogenic system. *Earth-Science Reviews*, *150*, 531–593. https://doi.org/10.1016/j.earscirev.2015.08.001

Zhang, Y., Anderson, N. S., Mohr, M. T., Nelson, L. L., Macdonald, F. A., Schmitz, M. D., et al. (2024a). Paleomagnetic Records From Pulsed Magmatism in the Southwestern Laurentia Large Igneous Province and Cardenas Basalt Support Rapid Late Mesoproterozoic Plate Motion [code repository]. *Zenodo*. https://doi.org/10.5281/ZENODO.10625968

Zhang, Y., Anderson, N. S., Mohr, M. T., Nelson, L. L., Macdonald, F. A., Schmitz, M. D., et al. (2024b). Paleomagnetic Records From Pulsed Magmatism in the Southwestern Laurentia Large Igneous Province and Cardenas Basalt Support Rapid Late Mesoproterozoic Plate Motion [*data repository*]. https://doi.org/10.7288/V4/MAGIC/20009

References From the Supporting Information

Fisher, N. I., Lewis, T., & Embleton, B. J. (1987). *Statistical analysis of spherical data*. Cambridge university press.

Haggerty, S. E., & Baker, I. (1967). The alteration of olivine in basaltic and associated lavas. *Contributions to Mineralogy and Petrology*, *16*(3), 233–257. https://doi.org/10.1007/bf00371094

Hedley, I. (1968). Chemical remanent magnetization of the FeOOH, Fe2O3 system. *Physics of the Earth and Planetary Interiors*, *1*(2), 103–121. https://doi.org/10.1016/0031-9201(68)90055-1

Heslop, D., & Roberts, A. P. (2018). Revisiting the paleomagnetic reversal test: A Bayesian hypothesis testing framework for a common mean direction. *Journal of Geophysical Research: Solid Earth*, *123*(9), 7225–7236. https://doi.org/10.1029/2018jb016081

Heslop, D., Scealy, J. L., Wood, A. T. A., Tauxe, L., & Roberts, A. P. (2023). A bootstrap common mean direction test. *Journal of Geophysical Research: Solid Earth*, *128*(8). https://doi.org/10.1029/2023jb026983

McClelland, E. (1987). Self-reversal of chemical remanent magnetization: A palaeomagnetic example. *Geophysical Journal International*, *90*(3), 615–625. https://doi.org/10.1111/j.1365-246x.1987.tb00744.x

Mcclelland, E., & Goss, C. (1993). Self reversal of chemical remanent magnetization on the transformation of maghemite to haematite. *Geophysical Journal International*, *112*(3), 517–532. https://doi.org/10.1111/j.1365-246x.1993.tb01185.x

McFadden, P., & McElhinny, M. (1990). Classification of the reversal test in palaeomagnetism. *Geophysical Journal International*, *103*(3), 725–729. https://doi.org/10.1111/j.1365-246X.1990.tb05683.x

Meert, J. G., Pivarunas, A. F., Evans, D. A., Pisarevsky, S. A., Pesonen, L. J., Li, Z.-X., et al. (2020). The magnificent seven: A proposal for modest revision of the quality index. *Tectonophysics*, *790*, 228549. https://doi.org/10.1016/j.tecto.2020.228549

Sun, S.-S., & McDonough, W. F. (1989). Chemical and isotopic systematics of oceanic basalts: Implications for mantle composition and processes. *Geological Society, London, Special Publications*, *42*, 313–345. https://doi.org/10.1144/gsl.sp.1989.042.01.19

Tauxe, L., Kylstra, N., & Constable, C. (1991). Bootstrap statistics for paleomagnetic data. *Journal of Geophysical Research*, *96*(B7), 11723–11740. https://doi.org/10.1029/91jb00572

Torsvik, T. H., Van der Voo, R., Preeden, U., Mac Niocaill, C., Steinberger, B., Doubrovine, P. V., et al. (2012). Phanerozoic polar wander, palaeogeography and dynamics. *Earth-Science Reviews*, *114*(3–4), 325–368. https://doi.org/10.1016/j.earscirev.2012.06.007

21699356, 2024, 10, Downloaded from https://agupubs.onlinelibrary.wiley.com/doi/10.1029/2024JB029036 by Yiming Zhang - University Of Minnesota Lib , Wiley Online Library on [19/10/2024]. See the Terms and Conditions (https://onlinelibrary.wiley.com/terms-and-conditions) on Wiley Online Library for rules of use; OA articles are governed by the applicable Creative Commons License